IMMUNOLOGY

4-1BB costimulation promotes CAR T cell survival through noncanonical NF-κB signaling

Benjamin I. Philipson[1,2,3], Roddy S. O'Connor[2], Michael J. May[4], Carl H. June[2], Steven M. Albelda[3], Michael C. Milone[2]*

Clinical response to chimeric antigen receptor (CAR) T cell therapy is correlated with CAR T cell persistence, especially for CAR T cells that target CD19$^+$ hematologic malignancies. 4-1BB–costimulated CAR (BBζ) T cells exhibit longer persistence after adoptive transfer than do CD28-costimulated CAR (28ζ) T cells. 4-1BB signaling improves T cell persistence even in the context of 28ζ CAR activation, which indicates distinct prosurvival signals mediated by the 4-1BB cytoplasmic domain. To specifically study signal transduction by CARs, we developed a cell-free, ligand-based activation and ex vivo culture system for CD19-specific CAR T cells. We observed greater ex vivo survival and subsequent expansion of BBζ CAR T cells when compared to 28ζ CAR T cells. We showed that only BBζ CARs activated noncanonical nuclear factor κB (ncNF-κB) signaling in T cells basally and that the anti-CD19 BBζ CAR further enhanced ncNF-κB signaling after ligand engagement. Reducing ncNF-κB signaling reduced the expansion and survival of anti-CD19 BBζ T cells and was associated with a substantial increase in the abundance of the most pro-apoptotic isoforms of Bim. Although our findings do not exclude the importance of other signaling differences between BBζ and 28ζ CARs, they demonstrate the necessary and nonredundant role of ncNF-κB signaling in promoting the survival of BBζ CAR T cells, which likely underlies the engraftment persistence observed with this CAR design.

INTRODUCTION

Chimeric antigen receptor (CAR) T cell therapy targeting CD19 has induced complete tumor regression in a large percentage of patients suffering from hematologic malignancies, especially in children and young adults with acute lymphoblastic leukemia (ALL) (*1*). Event-free survival after CD19-specific CAR T cell therapy is highly correlated with the kinetics of T cell expansion (increase in cell number) and the area under the concentration-time curve (AUC) for the first 28 days after adoptive transfer (*2*). Although loss of antigen or epitope remains the most frequent mechanism of resistance to this therapy (*3*), relapse within the first 6 months is associated with the early loss of CAR T cell engraftment, illustrating the importance of persistent T cell engraftment to the success of adoptive cell therapy approaches (*2*, *4*, *5*).

The persistence of CAR T cells in vivo over time after adoptive transfer is influenced by CAR design. CARs are transmembrane proteins consisting of an antibody single-chain variable fragment (scFv), a hinge connecting to a transmembrane domain, and one or more intracellular signaling domains (*6*). The most commonly used designs combine the T cell receptor (TCR) subunit CD3ζ with the intracellular domain of either of the costimulatory molecules, CD28 or 4-1BB. Comparing CAR T cell persistence across human clinical trials using 28ζ or BBζ CD19-specific CARs, although fraught with pitfalls due to the other differences in the CARs used or in T cell manufacturing (for example, scFv, gene transfer vector, or culture conditions), suggests the greater persistence of 4-1BB–costimulated CAR T cell engraftment relative to CD28-costimulated CAR T cells (*7*, *8*). This trend is more directly substantiated in murine adoptive transfer models, implying that costimulation directly affects CAR T cell persistence (*9*). When exchanged with CD28 costimulation, 4-1BB costimulation also rescues CAR T cell survival in the context of a basally signaling CAR (*10*), and basally signaling BBζ CAR T cells markedly expand ex vivo (*11*).

The signaling pathways that lead to the observed differences in CAR T cell persistence remain poorly understood. Salter *et al.* (*12*) demonstrated that 28ζ CARs drive both constitutive and CAR activation–induced proximal signaling through the kinases Lck and Zap-70 more potently than do the BBζ CARs. This potent proximal signaling promotes the terminal differentiation of 28ζ CAR T cells, which can be reversed by silencing two of the immunoreceptor tyrosine-based activation motif (ITAM) domains of the CD3ζ domain (*13*). This reversal suggests that CD28 signaling in the CAR is a dominant mechanism for the reduced persistence of these CAR T cells. However, 4-1BB costimulation enhances CAR T cell survival and persistence even in the context of the full 28ζ CAR signal (*14*, *15*). This enhancement is consistent with the nonoverlapping roles that these costimulatory receptors play in normal immunity, especially for CD8$^+$ T cell memory (*16*–*20*). Long-term CD8$^+$ T cell survival after viral infections is supported by specific tumor necrosis factor receptor superfamily (TNFRSF) members, including 4-1BB (*21*, *22*). Unlike CD28, a distinct property of these receptors, and one that was specifically observed in one report on murine 4-1BB, is the capacity to activate the noncanonical nuclear factor κB (ncNF-κB) pathway (*23*–*26*). Distinct from the classical NF-κB signaling pathway downstream of TCR and CD28 stimulation mediated by the CARMA1 complex and protein kinase Cθ (PKCθ) (*23*, *27*–*29*), the ncNF-κB pathway promotes cell survival in numerous contexts, including normal lymphoid development under the control of TNFRSF members (*30*–*32*), Epstein-Barr virus infection (*33*), and malignancy (*34*–*37*).

ncNF-κB signaling is a complex pathway with slower activation kinetics compared with that of classical NF-κB signaling. It is initiated by the stabilization of NF-κB–inducing kinase (NIK), which is Lys^{48} (K48)–polyubiquitylated by the E3 ubiquitin ligases cellular inhibitors of apoptosis 1 (cIAP1) and 2 (cIAP2) and constitutively

[1]Medical Scientist Training Program, Perelman School of Medicine of the University of Pennsylvania, Philadelphia, PA 19104, USA. [2]Department of Pathology and Laboratory Medicine, Perelman School of Medicine of the University of Pennsylvania, Philadelphia, PA 19104, USA. [3]Department of Medicine, Perelman School of Medicine of the University of Pennsylvania, Philadelphia, PA 19104, USA. [4]Department of Biomedical Sciences, University of Pennsylvania School of Veterinary Medicine, Philadelphia, PA 19104, USA.
*Corresponding author. Email: milone@pennmedicine.upenn.edu

degraded by the proteasome (*38*). Upon ligand-dependent TNFRSF trimerization, differential TNF receptor–associated factor (TRAF) recruitment shifts cIAP1/2-mediated K48 polyubiquitylation from NIK to TRAF3, thereby alleviating the continuous proteasomal degradation of NIK. NIK accumulates and coordinates a protein complex including inhibitor of NF-κB kinase α (IKKα) and the Rel homology domain family members RelB and p100, the latter two of which form a heterodimer that is basally sequestered in the cytoplasm. Accumulating NIK phosphorylates IKKα, which, in turn, phosphorylates p100, generating a phosphodegron that leads to the partial degradation of p100 by the proteasome to form p52. The newly formed RelB-p52 heterodimer then translocates to the nucleus where it mediates transcriptional control of numerous genes involved in lymphoid development (*38*) and, in cancer cells, synergizes with extracellular signal–regulated kinase (ERK) to suppress genes expressing the proapoptotic proteins Bim and Bcl-2-modifying factor (BMF) (fig. S1) (*35*). Similar to 4-1BB signaling, ncNF-κB signaling is also essential for T cell–mediated immunity. Memory T cells require ncNF-κB signaling to survive both in mice (*39*, *40*) and in humans; the latter requirement was revealed by a deficiency in long-lived memory T cells in two patients with biallelic, loss-of-function mutations in NIK (*32*). Similarly, mice deficient in NIK form few persistent memory T cells when challenged with acute lymphocytic choriomeningitis virus infection (*40*). Furthermore, T cell–specific NIK knockout mice have substantially fewer circulating memory T cells than their wild-type counterparts, suggesting that NIK supports T cell persistence through a cell-intrinsic mechanism (*39*).

On the basis of the importance of ncNF-κB signaling to T cell memory formation and the report of activation of this pathway by endogenous 4-1BB in murine T cells, we evaluated the activation and role of this pathway in human CAR T cells. We showed that ncNF-κB signaling played an essential role in supporting BBζ CAR T cell survival. In addition to providing greater insight into the costimulatory mechanisms of the CD28 and 4-1BB domains in CARs, the increased understanding of the role of this pathway in human T cells offers opportunities to manipulate it more broadly in T cell–based immunotherapies that rely upon T cell survival to mediate clinical benefit.

RESULTS

4-1BB costimulation enhances ex vivo CAR T cell expansion relative to CD28 costimulation and is associated with improved T cell survival

To study the ex vivo expansion of T cells after stimulation by CD19-specific CARs bearing different costimulatory domains, we used the approach of repeated in vitro stimulation (*13*–*15*, *41*). We added irradiated Nalm6 leukemic cells bearing the CD19 target antigen to mCherry-expressing 28ζ or BBζ CAR T cell cultures (fig. S2) at 7-day intervals (Fig. 1A). Similar to previous studies comparing CD28- and 4-1BB–costimulated CARs, T cells bearing a 4-1BB–costimulated CAR (BBζ CAR T cells) accumulated over 14 days to yield about 1-log more T cells than CD28-costimulated CAR T cells (28ζ CAR T cells) (Fig. 1B). This increased expansion was associated with improved viability, which we observed by a 14% (±3.2%) absolute reduction in T cells that acquired 7-aminoactinomycin D (7AAD) fluorescence and lost mCherry on day 14 for BBζ CAR T cells relative to 28ζ CAR T cells (Fig. 1C). To determine whether there was also a difference in relative proliferation, we measured the abundance of proliferating cell nuclear antigen (PCNA) by Western blotting (Fig. 1D) and found no statistically significant difference in PCNA

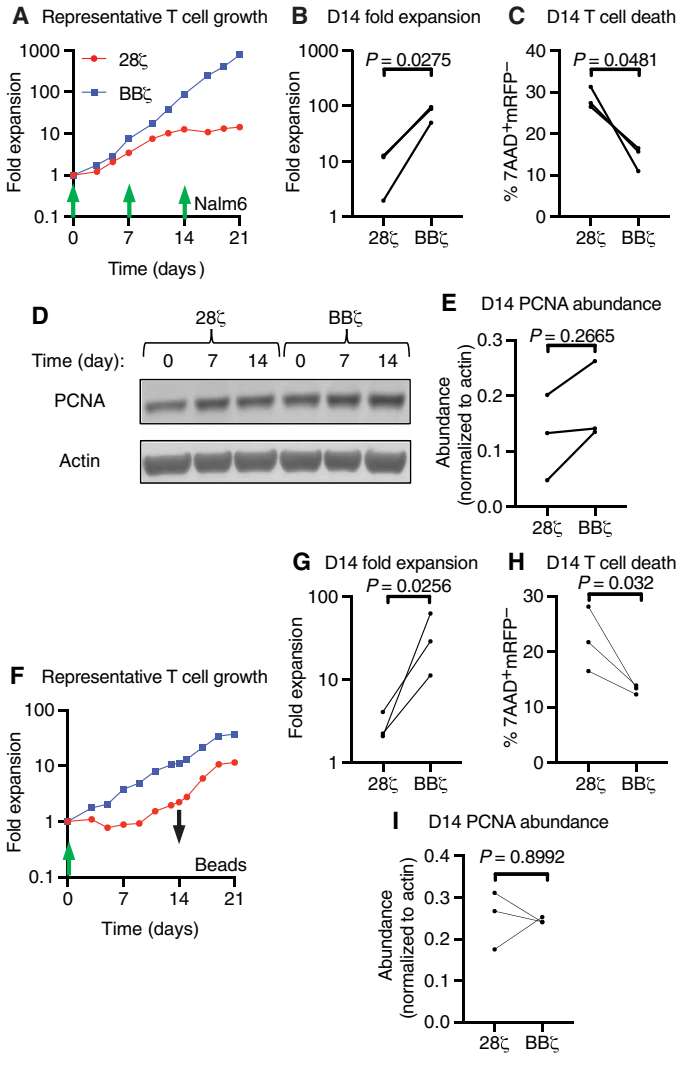

Fig. 1. 4-1BB–costimulated CAR activation drives greater ex vivo T cell expansion and survival than does CD28-costimulated CAR activation. (**A**) Representative ex vivo expansion of the indicated CAR T cells stimulated by irradiated Nalm6 target cells at the indicated times at a T cell to target cell ratio of 2:1. (**B**) Quantification of T cell expansion after 14 days of ex vivo culture from the experiments represented in (A). (**C**) Quantification of cell death by measurement of the percentage of $7AAD^{+}mCherry^{-}$ cells in all events collected on day 14 of ex vivo culture from the experiments represented in (A). (**D**) Representative Western blotting analysis of PCNA abundance in the indicated CAR T cells at 0, 7, and 14 days of ex vivo culture with Nalm6 target cells. (**E**) Quantification of the relative amounts of PCNA in the indicated CAR T cells on day 14 of ex vivo culture with Nalm6 target cells. Data in (B), (C), and (E) are from three donors in two independent experiments and were analyzed by paired Student's *t* test. (**F**) Representative ex vivo expansion of the indicated CAR T cells stimulated by anti-CD19 idiotype–coated target beads (at a T cell to bead ratio of 1:3) added at day 0 (green arrow) and removed at day 14 of culture (black arrow). (**G**) Quantification of T cell expansion after 14 days of ex vivo culture from the experiments represented in (F). (**H**) Quantification of cell death as assessed by measurement of the percentage of $7AAD^{+}mCherry^{-}$ cells in all events collected on day 14 of ex vivo culture from the experiments represented in (F). Data in (G) and (H) are from three donors in three independent experiments and were analyzed by paired Student's *t* test. (**I**) Quantification of the relative abundance of PCNA as assessed by Western blotting analysis of the indicated CAR T cells on days 0, 7, and 14 of ex vivo culture with target beads. Data are from donors in three independent experiments and were analyzed by paired Student's *t* test.

abundance between 28ζ and BBζ CAR T cells at day 0, 7, or 14 after CAR restimulation (Fig. 1E).

To identify signaling pathways that enhanced BBζ CAR T cell survival, we used a bead-based, artificial antigen-presenting cell (aAPC) approach for activating CD19-specific CAR T cells. We coated magnetic microbeads with anti-CD19 idiotype antibodies to cross-link the anti-CD19 CAR. This approach avoided the introduction of target cell proteins and RNA that confound analyses of signaling and did not add additional signals to the CAR T cells through other costimulatory interactions such as by integrin and CD28 activation (*42*). Furthermore, such beads have been used by our group and others to study CAR signaling and its effects on T cell expansion, metabolism, and differentiation (*12*, *43*, *44*). Similar to the studies using activation by Nalm6 leukemic cells, BBζ CAR T cells activated by these beads also expanded about a log more than did 28ζ CAR T cells (Fig. 1, F and G, and fig. S3). These expansions were less than those achieved with the irradiated target cells, likely due to a loss of additional costimulatory signals provided by those cells. Even so, we observed a 8.9% (±3.1%) absolute reduction in $7AAD^{+}mCherry^{-}$ cells on day 14 of BBζ CAR T cells relative to 28ζ CAR T cells (Fig. 1H) and did not detect a statistically significant difference in PCNA abundance (Fig. 1I). From these data, we conclude that our bead-based expansion system achieved similar outcomes as did the irradiated cell system.

CAR intracellular domains activate overlapping but kinetically and quantitatively distinct signaling pathways upon antigen stimulation

Both proximal and distal signaling pathways activated by the endogenous TCR and costimulatory molecules influence the proliferation and survival of T cells after CAR activation (*45*–*47*). To validate that our bead-based activation system stimulated similar T cell signaling pathways, we compared Zap-70, p65, and ERK1/2 phosphorylation in T cells expressing an anti-CD19 CAR containing no signaling domains (Δζ), the CD3 zeta chain alone (ζ), also known as a first-generation CAR, or one of two second-generation combinations, 28ζ or BBζ (fig. S4). Similar to recent work by Salter *et al.*, we observed that 28ζ CAR–mediated Zap-70 phosphorylation was 4.5-fold greater than that mediated by the BBζ CAR 12 hours after bead addition and 3.7-fold greater than that mediated by the ζ CAR 30 min after bead addition (Fig. 2, A and B). The phosphorylation of p65 at Ser^{536}, a measure of canonical NF-κB signaling, increased across all signaling CARs after bead addition, with a trend toward increased p65 phosphorylation early after activation of the 28ζ CAR and a small but statistically significant increase of 1.34-fold in the BBζ CAR T cells relative to that in the 28ζ CAR T cells at 12 hours (Fig. 2C). Also, like the work by Salter *et al.*, ERK1 and ERK2 phosphorylation both increased with activation of all signaling CARs over time (Fig. 2, D and E), with ERK2 phosphorylation increasing 2.2- and 1.9-fold by 28ζ and BBζ CAR activation, respectively, relative to that by ζ-only CAR activation at 30 min (Fig. 2E). We conclude from these data that the bead-based aAPC system activated anti-CD19 CARs, leading to CAR signaling in a similar manner to that reported in the literature (*12*, *43*), providing a robust system for evaluating signaling downstream of our CD19-specific CARs.

4-1BB, but not CD28, costimulation potentiates CAR-mediated ncNF-κB signaling

We hypothesized that the 4-1BB intracellular domain incorporated into a CAR specifically promoted CAR T cell survival and persistence

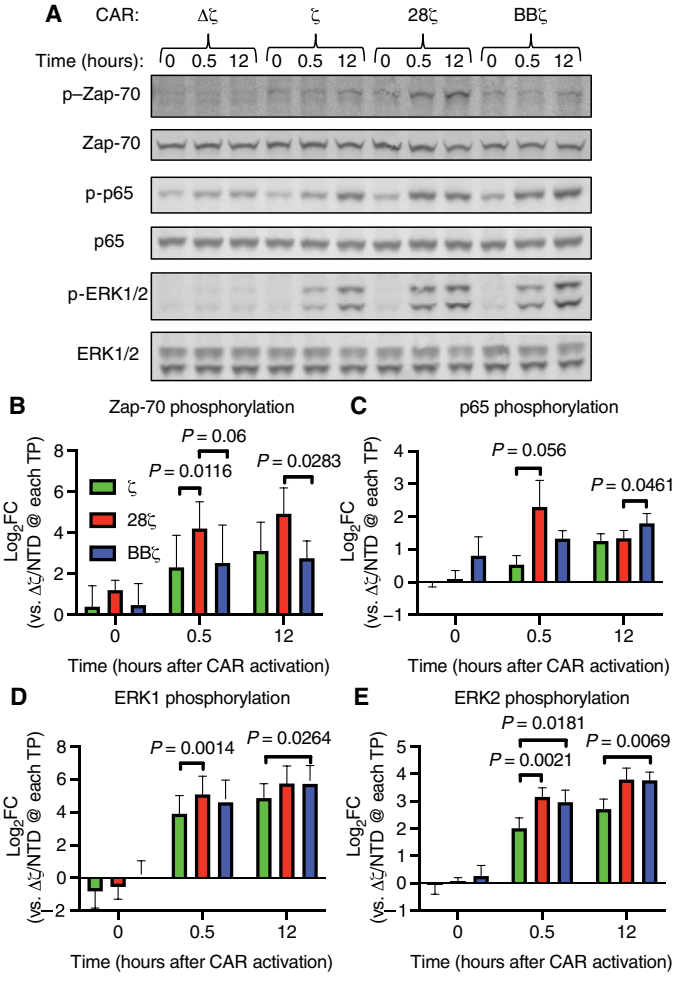

Fig. 2. Anti-CD19 idiotype target beads activate T cell signaling in anti-CD19 CAR T cells. (**A**) Representative Western blotting of total and phosphorylated Zap-70, p65, and ERK1/2 proteins before and at 30 min and 12 hours after the addition of anti-CD19 beads to the indicated CAR T cells at a bead–to–T cell ratio of 5:1. The anti-CD19 CAR T cells used expressed CARs with no signaling domain (Δζ), the CD3ζ chain intracellular domain alone (ζ), the CD28 and CD3ζ chain intracellular domains (28ζ), or the 4-1BB and CD3ζ chain intracellular domains (BBζ). (**B** to **E**) Quantification of the relative abundances of phosphorylated Zap-70 (B), p65 (C), ERK1 (D), and ERK2 (E) normalized to their respective total proteins from the experiments represented in (A). *P* values were determined by two-way ANOVA with Tukey's multiple comparisons test of data from three donors analyzed in three independent experiments. FC, fold change; TP, time point; NTD, non-transduced.

through activation of ncNF-κB signaling. To interrogate this pathway and establish optimal time points for comparison across CAR constructs, we first determined the kinetics of activation after engagement of the BBζ CAR (fig. S5, A to D). We measured ncNF-κB signaling using the commonly reported metrics of p100 processing, p100 phosphorylation (Fig. 3, A and B), and p52/p100 ratio (Fig. 3, A and C) (*48*). We found that p100 phosphorylation was statistically significantly increased after bead addition, peaking at 6.1-fold over baseline at 12 hours (Fig. 3B). Similarly, the p52/p100 ratio was statistically significantly increased over the first 12 hours after BBζ CAR activation, with a peak of 1.87-fold over baseline at 12 hours (Fig. 3C). The abundance of the initiator kinase for this pathway, NIK, was statistically significantly increased after BBζ CAR activation with a

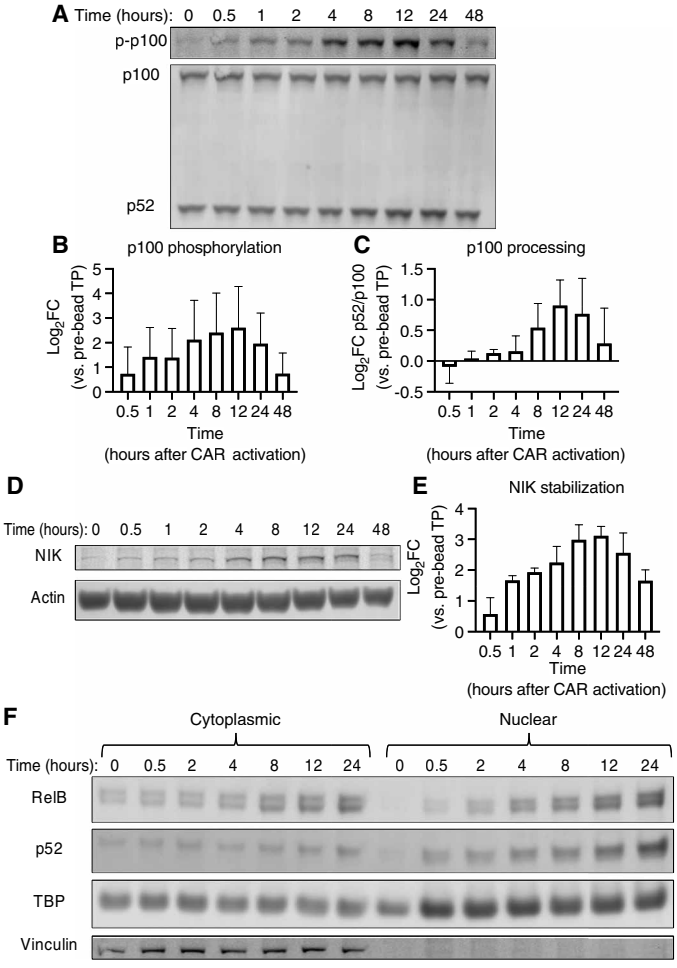

Fig. 3. 4-1BB–costimulated anti-CD19 CAR activation stimulates CAR T cell ncNF-κB signaling. (**A**) Representative Western blotting analysis of p100 phosphorylation and the processing of p100 to p52 at the indicated times before and after the addition of target beads to anti-CD19 BBζ CAR T cells. (**B** and **C**) Quantitative analyses of the relative amounts of phosphorylated p100 (B) ($P = 0.0397$ as determined by analyzing the data from two independent experiments using CAR T cells derived from three healthy donors by one-way ANOVA with the factor being time, as is the case for all of the P values in this figure) and the relative amounts of p52 generated by p100 processing (C) (p52/p100 ratio, $P = 0.0244$) from the experiments represented in (A). (**D**) Representative Western blotting analysis of NIK protein at the indicated times before and after target bead addition to anti-CD19 BBζ CAR T cells. Actin was used as a loading control. (**E**) Quantitative analysis of the relative amounts of NIK protein at the indicated times after the addition of beads to the cells in the experiments represented in (D) ($P = 0.011$). (**F**) Representative Western blotting analysis of the cytoplasmic and nuclear fractions from anti-CD19 BBζ CAR T cells before and at the indicated times after the addition of target beads. The blot is representative of two separate experiments using CAR T cells generated from two healthy donors (see fig. S6 for the other experiment).

peak of 8.7-fold over baseline also at 12 hours after CAR activation (Fig. 3, D and E). ncNF-κB signaling culminates in the nuclear translocation of RelB and p52. Therefore, we also measured RelB and p52 nuclear translocation in isolated nuclear fractions, as confirmed by loss of vinculin (Fig. 3F), at similar times after BBζ CAR activation using the same initial setup as for our assessment of NIK and p100 signal transduction. Cytoplasmic RelB increased and stayed above baseline after 8 hours of bead stimulation (Fig. 3F and fig. S5E), reflecting previously described increases in abundance after canonical NF-κB signaling (*49*). Furthermore, both RelB and p52 nuclear localizations were detectable before and increased after BBζ CAR activation (Fig. 3F and fig. S5E), indicating basal and ligand-induced activation of ncNF-κB signaling. Consistent with the delayed kinetics of this pathway relative to that of the canonical NF-κB pathway (*24*), we observed peak p100 processing and NIK stabilization 12 hours after BBζ CAR activation (Fig. 3, C and E).

To test the hypothesis that ncNF-κB signaling occurred solely in 4-1BB–costimulated CAR T cells, we compared ncNF-κB signaling by anti-CD19–targeted Δζ, ζ, 28ζ, or BBζ CARs before activation and at 30 min and 12 hours after bead addition. We found that p100 phosphorylation was 3.2-fold greater 12 hours after bead addition in BBζ CAR T cells relative to that in 28ζ CAR T cells (Fig. 4, A and B). We observed a similar trend in p100 phosphorylation when comparing the BBζ and ζ-only CAR T cells. The p52/p100 ratio was statistically significantly increased in BBζ CAR T cells relative to that in 28ζ CAR T cells at all times, including before activation (1.8-fold greater) and 12 hours afterward (2.4-fold greater), whereas no difference in the p52/p100 ratio was observed between the 28ζ and ζ-only CAR T cells (Fig. 4C). Although NIK stabilization was enhanced after BBζ CAR activation relative to after activation of the other CARs (Fig. 4D), this trend was not statistically significant (Fig. 4E). The downstream basal ncNF-κB signaling in BBζ CAR T cells relative to that in 28ζ CAR T cells was also reflected in increased baseline RelB nuclear occupancy (Fig. 4F and fig. S6), which was 1.3-fold greater in BBζ CAR T cells relative to that in the 28ζ CAR T cells (Fig. 4G). RelB nuclear translocation increased further 12 hours after CAR activation and was 5.4-fold greater in BBζ CAR T cells relative to that in 28ζ CAR T cells (Fig. 4G). Although we observed increased p52 nuclear occupancy in BBζ CAR T cells at all times relative to that in the ζ and 28ζ CAR T cells (Fig. 4F), this increase reached statistical significance for BBζ versus 28ζ CAR T cells only at the 30-min time point and for BBζ versus ζ CAR T cells only at the 12-hour time point (Fig. 4H).

To confirm the particular association between the BBζ CAR and ncNF-κB signaling in a CAR with an alternative scFv and antigen specificity (fig. S7), we compared the p52/p100 ratio in SS1-28ζ or SS1-BBζ CARs targeting mesothelin (fig. S7, A and C) before activation and at 30 min and 12 hours after the addition of mesothelin-coated beads (fig. S7, B and D to F). Similar to what we found with the CD19-specific CAR T cells, we observed a greater p52/p100 ratio in the SS1-BBζ CAR T cells compared to that in the SS1-28ζ CAR T cells from two separate donors before activation (fig. S7, E and F). Unlike in the anti-CD19 CAR T cells, the p52/p100 ratio decreased after the addition of mesothelin-coated beads to the SS1-BBζ CAR T cells, but it did not decrease in the SS1-28ζ CAR T cells under the same conditions. Together, these data suggest that the 4-1BB signaling domain within the CAR basally activates the ncNF-κB pathway regardless of the CAR target. Although the degree of antigen-induced enhancement of ncNF-κB signaling by BBζ CARs differs based on the scFv, nature of the ligand, or both, BBζ CAR T cells exhibited greater ncNF-κB signaling compared to that in 28ζ CAR T cells.

Expression of a dominant-negative NIK peptide reduces BBζ-mediated ncNF-κB signaling, ex vivo BBζ CAR T cell expansion, and survival

Targeting NIK has been a widely used strategy to block ncNF-κB signaling (*50*). Therefore, we used this approach to interrupt ncNF-κB

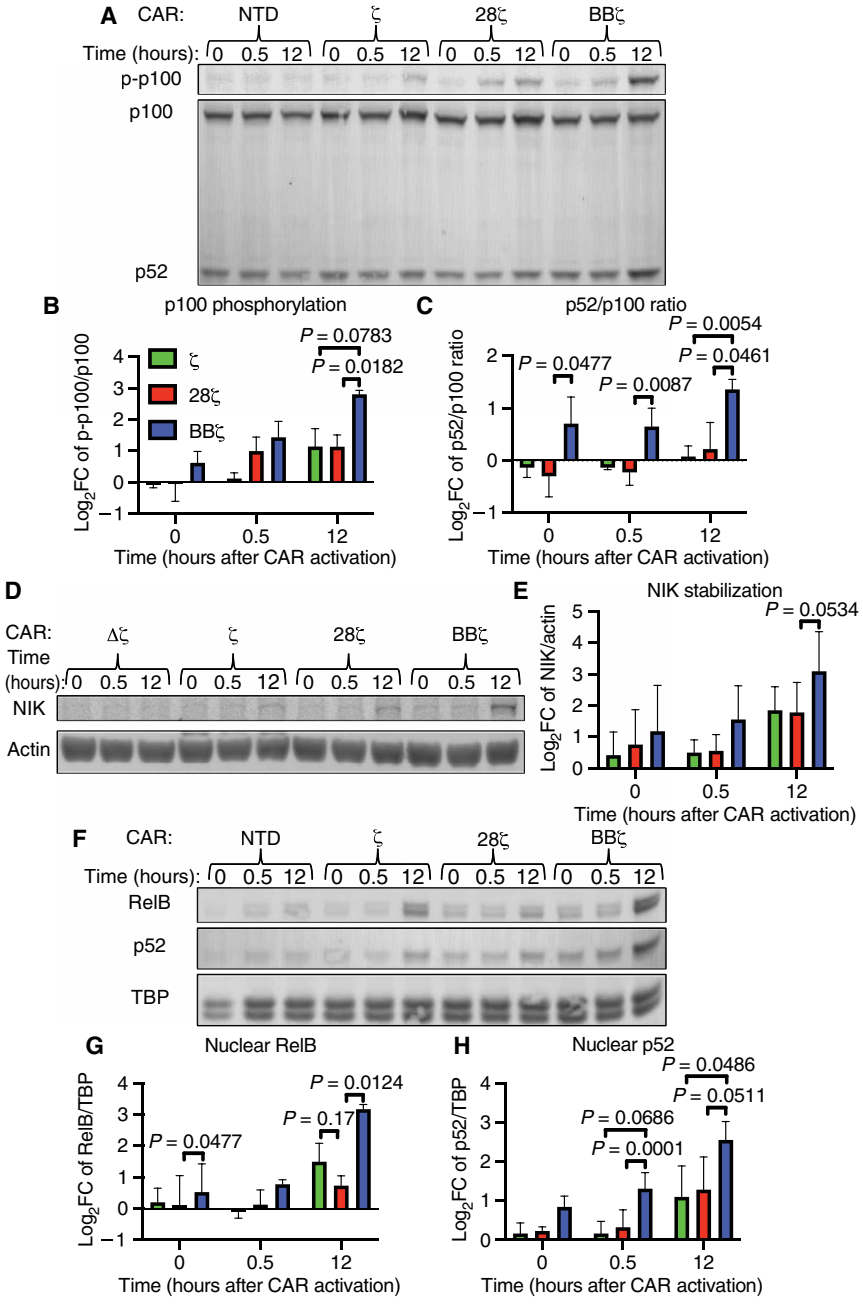

Fig. 4. 4-1BB, but not CD28, CAR costimulation drives basal and enhances CAR activation–induced ncNF-κB signaling. (**A**) Representative Western blotting analysis of the phosphorylation of p100 and of its processing to p52 in the indicated CAR T cells at the indicated times before and after the addition of target beads at a bead–to–T cell ratio of 5:1. The anti-CD19 CARs used had no signaling domain (Δζ), the CD3ζ chain intracellular domain alone (ζ, green), the CD28 and CD3ζ chain intracellular domains (28ζ, red), or the 4-1BB and CD3ζ chain intracellular domains (BBζ, blue). (**B** and **C**) Quantitative analyses of the relative abundances of phosphorylated p100 (B) and of the ratio of p52 to p100 (C) from the experiments represented in (A). (**D**) Representative Western blotting analysis of NIK protein in the indicated CAR T cells at the indicated times before and after the addition of target beads as described for (A). Actin was used as a loading control. (**E**) Quantitative analysis of relative amounts of NIK protein in the indicated cells from the experiments represented in (D). (**F**) Representative Western blotting analysis of RelB, p52, and TBP (loading control) in nuclear fractions from the indicated anti-CD19 CAR T cells before and at the indicated times after the addition of target beads as described for (A). (**G** and **H**) Quantitative analyses of the relative amounts of nuclear RelB (G) and nuclear p52 (H) in the indicated cells from the experiments represented in (F). Data in (B), (C), (E), (G), and (H) are from three donors in three independent experiments. All $\log_2$(fold change relative to nonsignaling group) quantifications of band fluorescence intensities were normalized to those of the loading control. *P* values reported were determined by two-way ANOVA with Tukey's multiple comparisons test.

signaling downstream of BBζ CAR activation by overexpressing the C terminus of NIK (dnNIK) in CAR T cells. dnNIK acts similarly to a dominant-negative mutant NIK protein by binding to p100 and thereby preventing downstream ncNF-κB signaling (*51*). Twenty-four hours after initially transducing primary human T cells with the BBζ CAR, we transduced the cells with either a control vector expressing mCherry alone or a bicistronic vector expressing dnNIK and mCherry. This strategy enabled us to compare ncNF-κB signaling in each group of cells by Western blotting analysis while maintaining equal CAR abundance across groups (fig. S8). We observed a 1.5-fold decrease in the p52/p100 ratio 12 hours after CAR activation in dnNIK-expressing T cells relative to that in control T cells (Fig. 5, A and B). Similarly, we observed 1.4- and 1.9-fold decreases in RelB nuclear occupancy 30 min and 12 hours, respectively, after BBζ CAR activation in dnNIK-expressing T cells relative to that in control T cells (Fig. 5, C and D, and fig. S9). We observed a similar trend in p52 nuclear occupancy, with statistically significant decreases of 1.9- and 2-fold at baseline and 12 hours after CAR activation, respectively, in dnNIK-expressing T cells relative to that in control T cells (Fig. 5, C and E, and fig. S9).

Having observed a reduction in ncNF-κB signaling as a result of dnNIK expression, we used this approach in the bead-based CAR T cell expansion model to test the hypothesis that ncNF-κB signaling mediated anti-CD19 4-1BB–costimulated CAR T cell survival. We observed that dnNIK-expressing BBζ CAR T cells expanded 3.1-fold less than did control BBζ CAR T cells after 14 days of exposure to anti-CD19 idiotype beads (Fig. 5, F and G). This reduction in expansion was associated with a 6.2% absolute increase in cell death as assessed by measurement of 7AAD uptake by flow cytometry on day 14 (Fig. 5H). We did not detect a significant difference in PCNA expression between control and dnNIK-expressing BBζ CAR T cells before or 14 days after CAR T cell activation (fig. S10, A and B). To exclude the possibility that dnNIK nonspecifically caused CAR T cell death after CAR activation, we conducted these studies with anti-CD19 28ζ CAR T cells in parallel (Fig. 5, I to K). We observed no statistically

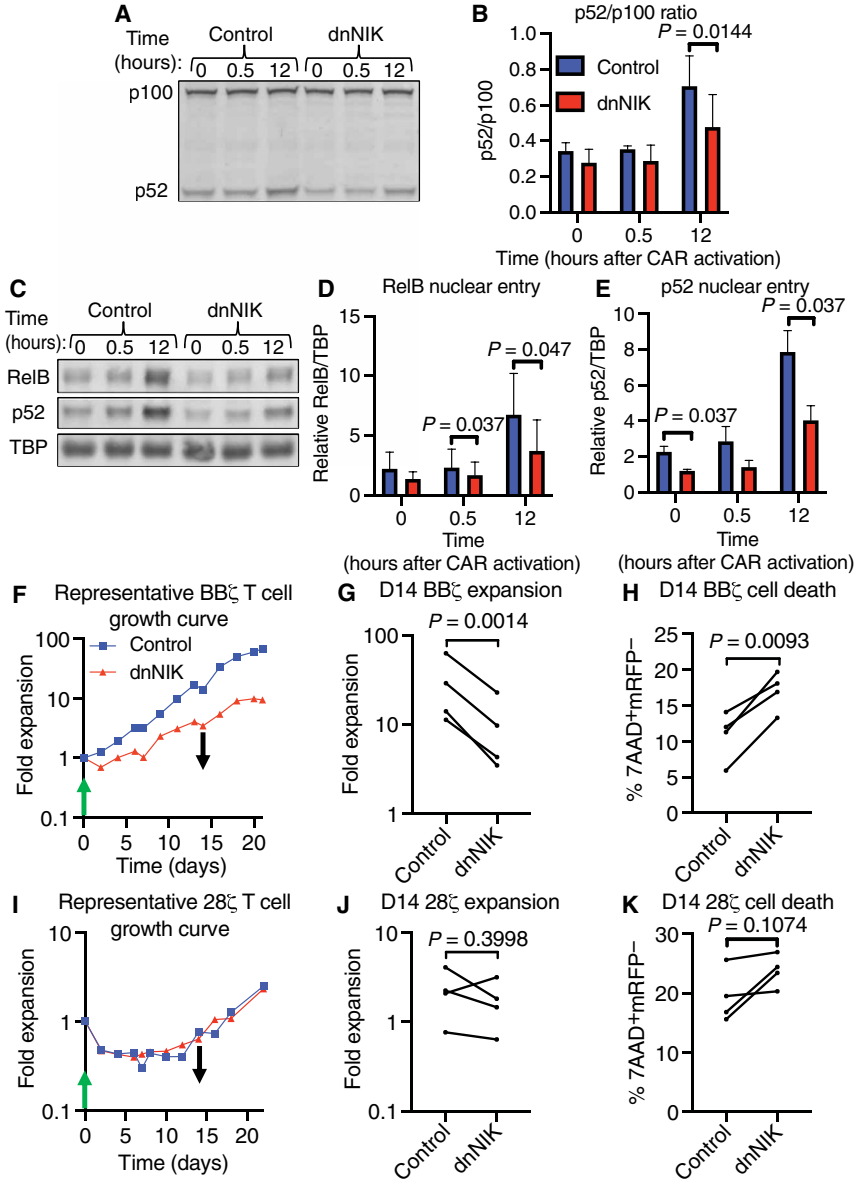

Fig. 5. Reducing 4-1BB costimulation–mediated ncNF-κB signaling diminishes BBζ CAR T cell ex vivo expansion and survival. (**A**) Representative Western blotting analysis of p100 processing to p52 before, 30 min, and 12 hours after the addition of target beads to anti-CD19 BBζ CAR T cells expressing either mCherry (control) or mCherry and dnNIK. (**B**) Quantitative analysis of the ratio of p52 to p100 ratio from the experiments represented in (A). Data are from CAR T cells generated from three donors in three independent experiments. *P* value was determined by two-way ANOVA with Holm-Sidak's multiple comparisons test. (**C**) Representative Western blotting analysis of RelB, p52, and TBP (loading control) in nuclear fractions of anti-CD19 BBζ CAR T cells treated as described for (A). (**D** and **E**) Quantitative analyses of the nuclear localization of RelB (D) and p52 (E) in cells from the experiments represented in (C) using TBP as the loading control. Data are from two independent experiments of CAR T cells generated from three donors. *P* values were determined by two-way ANOVA with Holm-Sidak's multiple comparisons test. (**F**) Representative ex vivo expansion of control or dnNIK-expressing BBζ CAR T cells stimulated by anti-CD19 idiotype–coated target beads (at a T cell–to–bead ratio of 1:3) and added at day 0 (green arrow) and removed at day 14 of culture (black arrow). (**G**) Quantification of T cell expansion after 14 days of ex vivo culture from the experiments represented in (F). (**H**) Quantification of cell death by measurement of the percentage of $7AAD^+mCherry^-$ cells in all events collected on day 14 of the ex vivo culture represented in (F). (**I**) Representative ex vivo expansion of control or dnNIK-expressing 28ζ CAR T cells stimulated by anti-CD19 idiotype–coated target beads at a T cell–to–bead ratio of 1:3 and added at day 0 (green arrow) and removed at day 14 of culture (black arrow). (**J**) Quantification of T cell expansion after 14 days of ex vivo culture from the experiments represented in (I). (**K**) Quantification of cell death by measurement of the percentage of $7AAD^+mCherry^-$ cells in all events collected on day 14 of the ex vivo culture represented in (I). All *P* values were determined by paired Student's *t* tests of data from four donors in four independent experiments.

significant differences in cell expansion (Fig. 5, I and J), 7AAD uptake (Fig. 5K), or PCNA abundance (fig. S10, C and D) between control and dnNIK-expressing 28ζ CAR T cells on day 14 of culture. These data indicate that 4-1BB–costimulated anti-CD19 CAR T cells specifically require ncNF-κB signaling to promote cell survival.

4-1BB costimulation–mediated ncNF-κB signaling represses the pro-apoptotic protein Bim

ncNF-κB signaling in multiple myeloma cell lines and 4-1BB costimulation in T cells both lead to enhanced cell survival by suppressing the production of the pro-apoptotic protein Bim (*35*, *52*, *53*). From our observation that ncNF-κB signaling supported BBζ CAR T cell survival, we hypothesized that the increased cell death observed in dnNIK-expressing BBζ CAR T cells was due, at least in part, to increased Bim abundance. To test this hypothesis, we assessed Bim abundance by Western blotting analysis at baseline and 14 days after the addition of anti-CD19 idiotype beads to CD19-specific BBζ (Fig. 6, A to E, and fig. S11, A to C) and 28ζ (Fig. 6, F to J, and fig. S11, D to F) CAR T cells transduced with a dnNIK-expressing vector or a control vector. No statistically significant difference was detected in the amounts of any of the Bim isoforms at baseline between dnNIK-expressing and control CAR T cells expressing either the BBζ (Fig. 6, B and C, and fig. S11B) or 28ζ (Fig. 6, G and H, and fig. S11E) CARs. The abundance of Bim_L was statistically significantly greater in dnNIK-expressing BBζ cells than in BBζ cells at day 14 (Fig. 6D), with a similar trend observed for Bim_S (Fig. 6E). No statistically significant differences in the abundances of any of the isoforms of Bim were apparent between dnNIK-expressing 28ζ CAR T cells and control vector–expressing 28ζ CAR T cells at day 14 (Fig. 6, I and J, and fig. S11F). Comparing Bim isoform abundances between 28ζ and BBζ CAR T cells at baseline (Fig. 6, K and L, and fig. S11, G and H) revealed a statistically significant decrease in Bim_S abundance in the BBζ cells with a similar trend observable for Bim_L (Fig. 6, K and L). Together, these observations of differential Bim isoform abundance before CAR activation between 28ζ and BBζ CAR T cells,

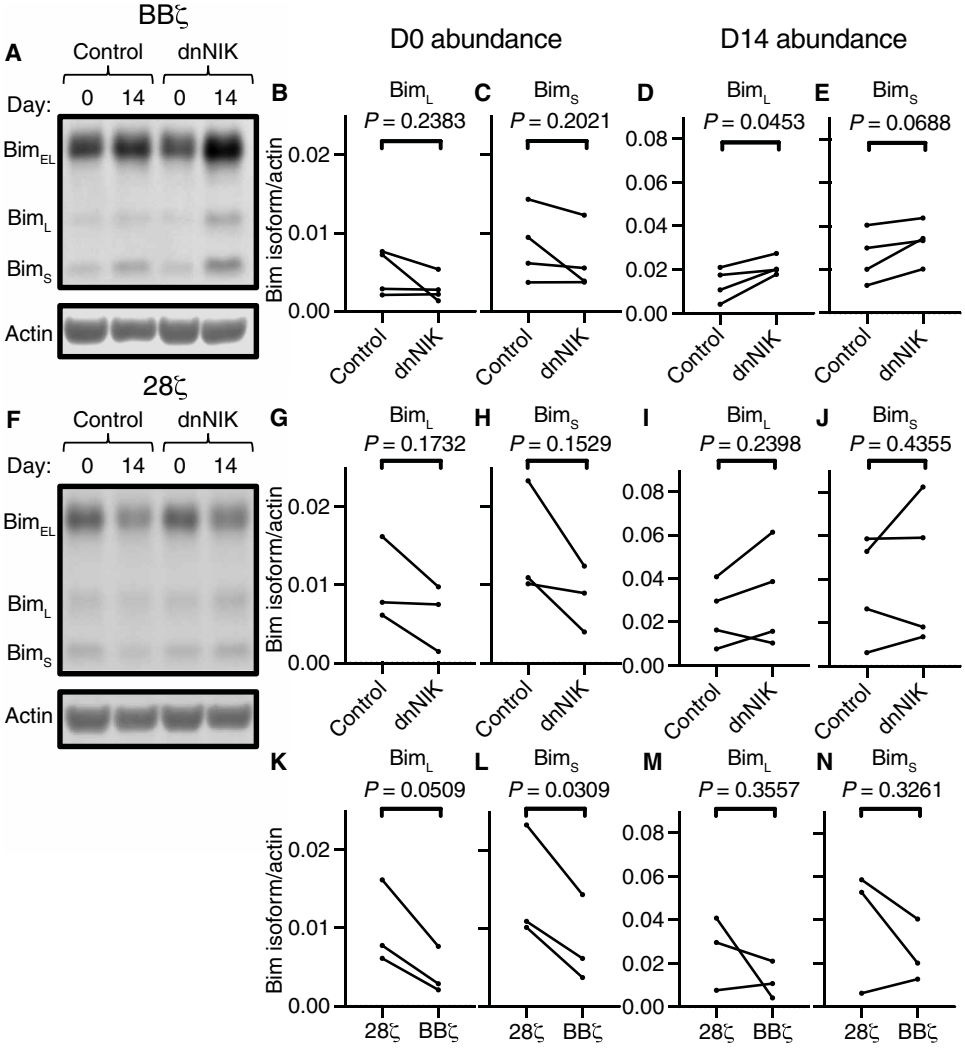

Fig. 6. 4-1BB costimulation–mediated ncNF-κB signaling opposes expression of the pro-apoptotic protein Bim. (**A**) Representative Western blotting analysis of Bim isoforms in control and dnNIK-expressing BBζ CAR T cells before and 14 days after ex vivo expansion in response to the addition of beads. (**B** to **E**) Quantitation of the relative basal amounts of Bim_L (B) and Bim_S (C), as well as of the amounts of Bim_L (D) and Bim_S (E) 14 days after the addition of beads from the experiments represented in (A). Data in (B) to (E) are from four donors in four independent experiments. All *P* values were derived from paired Student's *t* tests. (**F**) Representative Western blotting analysis of Bim isoforms in control or dnNIK-expressing 28ζ CAR T cells before and 14 days after ex vivo expansion in response to the addition of beads. (**G** and **H**) Quantitation of the relative basal amounts of Bim_L (G) and Bim_S (H) from the experiments represented in (F). Data are from three independent experiments with three donors. *P* values were derived from paired Student's *t* tests. (**I** and **J**) Quantitation of the relative amounts of Bim_L (I) and Bim_S (J) 14 days after bead addition from the experiments represented in (F). Data in (I) and (J) are from four donors in four independent experiments. No pre-bead sample was taken for fourth donor shown in (I) and (J). *P* values were derived from paired Student's *t* tests. (**K** and **L**) Comparison of the basal amounts of Bim_L (K) and Bim_S (L) between 28ζ and BBζ CAR T cells. (**M** and **N**) Comparison of the relative amounts of Bim_L (M) and Bim_S (N) between 28ζ and BBζ CAR T cells 14 days after expansion in response to beads. Data in (K) to (N) are from three donors in three independent experiments. All *P* values were derived from paired Student's *t* tests.

especially with respect to the low amounts of Bim_S in BBζ cells and the increase in Bim isoform abundance in the context of dnNIK-expressing cells after CAR activation, are consistent with *bcl2l11* (which encodes Bim) or its products as a target of ncNF-κB signaling in BBζ CAR T cells. The failure to detect a difference in Bim isoform abundance when ncNF-κB signaling was disrupted by the presence of dnNIK before CAR activation may be a result of the low overall amounts of Bim_S and Bim_L.

Although previous work with multiple myeloma cell lines demonstrated cooperative suppression of Bim production by ERK and ncNF-κB signaling (*35*), previous studies of T cells have only addressed ERK-mediated Bim suppression (*53*–*55*). Therefore, we assessed ERK phosphorylation in the dnNIK-expressing BBζ CAR T cells to determine whether dnNIK expression affected BBζ CAR–mediated ERK activation. Thirty minutes after bead addition, we observed a 1.2-fold reduction in ERK1 phosphorylation in dnNIK-expressing CAR T cells relative to that in control cells but saw no statistically significant difference in ERK1 phosphorylation before or 12 hours after bead addition (fig. S12, A and B). We also observed no statistically significant difference in ERK2 phosphorylation at any time (fig. S12C). Thus, although the reduction in ERK1 phosphorylation upon activation in dnNIK-expressing CAR T cells was small and transient, we cannot completely rule out that the observed reductions in Bim abundance are not, in part, due to small reductions in ERK signaling.

Another transcription factor known to drive Bim abundance in T cells is Forkhead box O3a (FOXO3a) (*56*). FOXO3a is regulated by numerous signaling pathways, including by γ-chain cytokines through phosphorylation of Thr^{32} and subsequent proteasomal degradation (*56*, *57*). To determine whether γ-chain cytokine signaling was affected by dnNIK and affected Bim abundance through FOXO3a regulation, we assessed FOXO3a phosphorylation at Thr^{32} and total FOXO3a abundance in control and dnNIK-expressing BBζ CAR T cells at days 0 and 14 of expansion (fig. S13, A and B). We observed no statistically significant differences in FOXO3a abundance between the control and dnNIK-expressing cells at either time (fig. S13B), instead observing a reduction in the amount of FOXO3a from days 0 to 14. We were also unable to detect any phosphorylation of FOXO3a at Thr^{32} in any of the samples (fig. S13A). Instead, we detected the phosphorylation of FOXO1 at Thr^{34}, which can be distinguished by its smaller size relative to that of FOXO3a in Western blotting analysis (fig. S13A). From these data, we conclude that FOXO3a was unaffected by dnNIK and is unlikely to contribute to changes in Bim abundance.

DISCUSSION

Here, we showed that the 4-1BB cytoplasmic domain incorporated into a CAR potently activates ncNF-κB signaling in human T cells.

This activation appeared to be constitutive across two 4-1BB–costimulated CARs with independent antigenic specificity, and ncNF-κB signaling was also increased in CD19-specific BBζ CAR T cells upon CAR engagement with ligand when compared with that in T cells expressing a first-generation CAR or a CD28-costimulated CAR. Moreover, disruption of this pathway substantially impaired anti-CD19 BBζ CAR T cell survival after CAR-mediated activation, leading to reduced T cell expansion ex vivo. This reduced expansion and survival was associated with the increased abundance of the pro-apoptotic protein Bim, the suppression of which mediates the prosurvival effects of ncNF-κB signaling in other systems (*35*, *52*). Thus, we have demonstrated that the 4-1BB costimulatory domain within a CAR directly promotes T cell survival through the ncNF-κB pathway, consistent with previous reports demonstrating that murine endogenous 4-1BB costimulation activates the ncNF-κB signaling (*24*), whereas endogenous CD28 costimulation does not (*23*, *58*). Our findings also add to our understanding of CAR costimulation because previously published reports have implicated faster and more potent proximal signaling by CD28-costimulated CARs to explain the differences between 4-1BB– and CD28-costimulated CAR T cell survival (*12*), whereas our results provide an additional mechanism directed by the 4-1BB domain itself.

A frequently observed feature of 4-1BB–costimulated CARs is basal signaling in the absence of antigen, so-called tonic signaling (*11*, *41*, *59*). Our data are consistent with these previous reports, and we also observed CD28-costimulated CAR basal signaling through the Zap-70 pathway (Fig. 2, A and B) (*12*). 4-1BB–costimulated CAR basal signaling appeared to occur through both the canonical NF-κB (Fig. 2) (*60*) and ncNF-κB (Figs. 3 and 4 and fig. S7) pathways, with the latter assessed by the detection of increased baseline p100 processing (Fig. 4C and fig. S7, E and F) and RelB nuclear localization (Fig. 4G). This basal ncNF-κB signaling is consistent across anti-CD19 and anti-mesothelin CARs. Note that not all pathways downstream of CAR activation were basally active. ERK phosphorylation was undetectable before CAR activation (Fig. 2, A, D, and E), and ERK2 phosphorylation, specifically at 30 min after CAR activation, was statistically significantly increased in both 4-1BB– and CD28-costimulated CAR T cells compared to that in first-generation CAR T cells (Fig. 2E). These distinct signaling modalities of CARs may arise from the constitutive dimerization of the CAR caused by disulfide bridges between the CD8 hinge domains or associations between neighboring scFv domains (*61*, *62*). Although native 4-1BB can form dimers linked by disulfide bonds (*63*), trimerization by its ligand 4-1BBL initiates downstream signaling (*63*–*67*). Whereas CD28-costimulated CAR basal signaling is detrimental to CAR T cell function and persistence (*10*, *68*), basal ncNF-κB signaling enhances the survival of multiple cell types, including T cells (*37*, *52*). These observations are consistent with the BBζ CAR–associated enhanced survival of both anti-CD19 (*2*, *41*) and anti-mesothelin (*69*) CAR T cells. ncNF-κB signaling integrates with ERK and other signaling pathways to achieve these effects (*35*, *70*–*73*), emphasizing the importance of further understanding how CARs activate some pathways in the absence of antigen and others only upon crosslinking, and how these signals combine to affect T cell function.

Whereas the basal activation of ncNF-κB signaling was consistent between two CARs with different scFv domains and antigen specificity, the observed difference in ligand-induced enhancement of the pathway between the CD19-specific and mesothelin-specific CARs was unexpected. We previously reported on the greater tonic signaling of the mesothelin-specific BBζ CAR incorporating the SS1 scFv as compared to that of CARs incorporating the anti-CD19 FMC63 scFv (*11*). Although speculative, this increased tonic signaling may lead to increased basal ncNF-κB signaling that is closer to the maximal response, thereby blunting our ability to see a difference upon activation. In this case, the small reduction that we observed in the p52/p100 ratio after bead-based activation could be the result of increased p100 abundance due to increased canonical NF-κB signaling (*60*, *74*). Alternatively, differences in the way that the CAR engages antigen or in the way that the antigen is presented for these two scFv-ligand systems might also influence the ligand-dependent activation of the ncNF-κB pathway downstream of a BBζ CAR. In particular, CARs internalize after antigen engagement, similarly to the TCR-CD3 complex, and the degree of internalization has been associated with ligand density and receptor affinity, which were not controlled in our activation system (*75*, *76*). This internalization can negatively affect CAR function (*76*) and could lead to diminished ncNF-κB signaling.

It is likely that the signaling downstream of 4-1BB costimulation that we observed will extend to other TNFRSFs. Transient expression of OX40L on both activated CD4 and CD8 T cells (*77*, *78*) can activate OX40 and downstream ncNF-κB signaling (*79*). This OX40-OX40L interaction may explain the small increase in ncNF-κB signaling that we observed in the ζ-chain and 28ζ CARs (Fig. 4) because both OX40 and OX40L are expressed at the cell surface upon T cell activation (*77*). Other researchers have incorporated OX40 costimulation directly into the CAR, thereby achieving enhancements in CAR T cell function and persistence (*80*), likely, at least in part, by activation of ncNF-κB signaling.

Approaches to pharmacologically activate the ncNF-κB pathway may also have utility, especially in T cell–based immunotherapies that do not use TNFRSF-based costimulation. One class of molecules, SMAC mimetics, has already been leveraged in combination with CAR T cells to enhance target-negative tumor cell killing (*81*). SMAC mimetics activate ncNF-κB signaling (*82*) and enhance T cell expansion and function (*83*). On the basis of our observations that 4-1BB costimulation–mediated ncNF-κB signaling is a driver of anti-CD19 CAR T cell survival, it may be possible to use SMAC mimetics to similarly enhance non-TNFRSF–costimulated T cells. This combination may be especially beneficial in transgenic TCR–directed T cell therapies, which have no synthetic costimulation (*84*). The tumor responses induced by these therapies correlate with cell persistence (*85*), which, based on our findings and previous reports of the effects of SMAC mimetic on T cells (*83*, *86*), could be increased by SMAC mimetic–mediated ncNF-κB signaling.

Last, our study has provided some insight into the mechanism by which ncNF-κB signaling by the 4-1BB domain of the CAR promotes T cell survival. The pro-apoptotic protein Bim plays a central role in T cell survival, is increased in abundance with T cell activation, and is repressed by ERK signaling (*87*–*92*). ERK-mediated Bim suppression was previously identified as a key mechanism by which endogenous murine 4-1BB enhances T cell survival (*53*); however, ncNF-κB signaling is implicated with ERK signaling in Bim regulation within multiple myeloma, suggesting that these two pathways are not mutually exclusive (*35*). In particular, ERK influences the cellular abundance of Bim in at least two ways: cooperation with RelB-p52 dimers to inhibit *bcl2l11* transcription (*35*) and through the phosphorylation and subsequent degradation of the Bim_{EL} isoform (*54*, *93*). This latter function of ERK may explain

why we did not observe differences in Bim_{EL} abundance between anti-CD19 28ζ and BBζ CAR T cells or between dnNIK-expressing BBζ CAR T cells and their controls (fig. S11), given that ERK was active in both settings (Fig. 2, D and E, and fig. S12) (*12*). The observed increases in Bim_L and Bim_S abundances in dnNIK-expressing BBζ CAR T cells relative to those in control cells after CAR activation (Fig. 6, D and E) are consistent with a transcriptional effect. In addition, the Bim_L and Bim_S isoforms are even more potent sensitizers of cells to apoptosis than is Bim_{EL} (*94*) and are capable of diminishing T cell survival in the absence of Bim_{EL} (*95*). We were unable to detect a difference in the amounts of Bim_L and Bim_S between anti-CD19 28ζ and BBζ CAR T cells after CAR-mediated expansion, despite showing baseline differences, which may be due to selection events occurring in the 28ζ CAR T cell culture as was observed with the early loss of cells upon bead stimulation (Fig. 5I) and consistent with previous work describing rapid 28ζ CAR T cell effector differentiation and cell loss (*12*, *43*). Bim suppression is an important downstream effect of 4-1BB–induced ncNF-κB signaling and likely contributes to BBζ CAR–mediated T cell survival, and further studies are needed to identify additional ncNF-κB–responsive genes that may also contribute to this survival.

Our system enabled us to identify ncNF-κB signaling as a specific and critical mediator of 4-1BB–costimulated CAR T cell survival, but we must also acknowledge some of its limitations. In this report, we focused on anti-CD19 CARs, which our group (*41*, *96*) and Salter *et al.* (*12*, *44*) have used to study CAR signaling. Although it is possible that our findings regarding CAR T cell survival are limited to the anti-CD19 CAR, 4-1BB–costimulated CAR T cells targeting multiple other antigens have been described as having similar enhanced survival (*69*, *97*–*99*). We overexpressed the C terminus of NIK to inhibit ncNF-κB signaling for our studies due to the well-described effects of this approach in disrupting ncNF-κB (*51*) and the lack of commercially available pharmacological inhibitors (*100*). Although protein overexpression and dominant-negative mutants can have unintended, off-target effects, the absence of an appreciable effect of dnNIK expression on both polyclonal T cell expansion in response to anti-CD3/anti-CD28 beads or 28ζ CAR–mediated expansion supports the generally nontoxic and targeted nature of our approach (Fig. 5, I and J).

In summary, we have identified an essential and nonredundant mechanism by which 4-1BB costimulation within a CAR supports T cell survival, namely, by mediating both basal and ligand-dependent activation of ncNF-κB signaling, which is associated with the reduced abundance of the most pro-apoptotic isoforms of Bim. ncNF-κB signaling by 4-1BB–costimulated CARs also likely influences gene expression in CAR T cells beyond those genes that affect survival and persistence because this pathway regulates the expression of many genes, such as those encoding chemokines and cytokines that are important for T cell trafficking and function (*38*). Although not evaluated in our study, ncNF-κB signaling has been reported to be required for the production of granulocyte-macrophage colony-stimulating factor (GM-CSF) by T helper 17 (T_H17) cells (*101*), suggesting that the 4-1BB–induced activation of this pathway could play a role in cytokine release syndrome that depends on this cytokine (*102*, *103*). Our work therefore represents only a beginning for the study of this unique and complex signaling pathway in CAR T cells that clearly deserves further exploration.

MATERIALS AND METHODS

Primary cells and Nalm6 cells

Primary human T cells were procured and cultured as described previously (*41*). Briefly, peripheral blood mononuclear cells were collected from anonymous healthy donors by aphaeresis. T cells were isolated from these aphaeresis products by the University of Pennsylvania Human Immunology Core using Lymphoprep and RosetteSep Human T Cell Enrichment Cocktail kits (STEMCELL Technologies) according to the manufacturer's instructions. Primary human T cells were cultured at 37°C in RPMI 1640 medium (Gibco) supplemented with 10% fetal bovine serum, 10 mM Hepes, penicillin (100 U/ml), and streptomycin (100 μg/ml). Nalm6 cells (American Type Culture Collection) were cultured at 37°C in the same medium that was used for T cells and refed every other day to a concentration of 0.25×10^6 cells/ml. Immediately before being used as stimulator cells, Nalm6 cells were irradiated with 100 Gy using an x-ray irradiator.

Generation of high-titer lentiviral vectors and T cell transduction

All CAR constructs were constructed as previously described (fig. S14) (*41*, *96*). All lentiviral vectors were produced and used to transduce primary human T cells for all single transduced T cell assays as previously described (*41*). Dual-transduced CAR T cells were generated as follows. We transduced T cells with anti-CD19 CARs containing either CD28 or 4-1BB costimulatory domains from healthy donor bulk T cells by lentiviral transduction, as described previously (*41*). These cells were subsequently transduced a second time with either a control lentiviral vector expressing mCherry or a bicistronic vector expressing dnNIK and mCherry, which were separated in the vector by a T2A site. These dual-transduced cells were cultured for 5 to 8 days, sorted to purity based on the abundance of mCherry, and further expanded with interleukin-7 (IL-7) and IL-15 (final concentration of 10 ng/ml; premium grade, Miltenyi Biotec) added with R10 medium every other day to maintain a starting concentration of 0.75×10^6 cells/ml. This expansion regimen was maintained until the average cell volume plateaued, as measured on a Coulter Counter (Beckman Coulter) for two consecutive measurements. These cells were either immediately used in assays (described as "fresh") or cryopreserved as described previously (*41*). Cells were enumerated by combining counts collected on a Coulter Counter (Beckman Coulter) with viability as assessed by flow cytometry using 7AAD (Cell Viability Solution, BD Via-Probe) exclusion (fig. S15A). CD4 (BUV395, RPA-T4, BD Biosciences), CD8 (BV785, RPA-T8, BioLegend), and CD19 (APC, HIB19, STEMCELL Technologies) cell surface expression were also assessed by flow cytometry. Elimination of irradiated Nalm6 stimulator cells by day 3 after addition was confirmed by the absence of $CD19^+$ cells (fig. S15B).

Preparation and use of stimulation beads

Stimulator beads were prepared as described previously (*43*). Briefly, Dynabeads M-450 Tosylactivated (Invitrogen) were washed and resuspended in a borate buffer (pH 9.5) at 4×10^8 beads/ml and then incubated overnight with 150 μg of anti-CD19 idiotype antibody (Novartis) or mesothelin-Fc at 37°C with constant mixing. The beads were then washed three times in wash buffer [3% human AB serum, 0.1% sodium azide, and 2 mM EDTA in phosphate-buffered saline (PBS)] at 4°C for 10 min each with constant mixing, followed by an overnight wash at 4°C in the same buffer with constant mixing. Before use, the beads were washed three times in PBS and then resuspended in

RPMI 1640–based medium as described earlier. Before use in experiments, the beads were subjected to quality control by being mixed with BBζ CAR T cells at a 3:1 bead-to-cell ratio. Bead activity was assessed by measuring T cell size with a Coulter Counter after 3 days and comparing it to the size of the same BBζ CAR T cells mixed with previous batches of beads at the same ratio used in parallel as a positive control, as well as to the size of BBζ CAR T cells cultured alone as a negative control. Beads were then used at a 3:1 bead-to-cell ratio for all bead-based expansion assays, whereas they were used at a 5:1 bead-to-cell ratio for all signaling assays. T cells for expansion assays were mixed with beads and cultured as described earlier. T cells for stimulation assays were mixed with beads and spun down to synchronize bead-cell contact. They were then incubated at 37°C for the times indicated in the figure legends.

Whole-cell lysis

Radioimmunoprecipitation assay (RIPA) buffer stock was made at 1× consisting of 150 mM NaCl, 1% NP-40, 0.5% deoxycholate, 0.1% SDS, and 50 mM tris-HCl (pH 8.0). The stock was stored at 4°C. The night before use, one tablet each of phosphatase inhibitor (PhosSTOP, Roche) and proteasome inhibitor (cOmplete, Roche) was added to a working volume of RIPA buffer. On the day of lysate collection, T cells were harvested from the culture, washed with ice-cold PBS (Corning), and resuspended in the working stock of ice-cold RIPA buffer. Lysates were incubated on ice for 30 min while being vortexed at maximum speed for 10 s at 10-min intervals. The cells were then centrifuged at 16,000*g* for 10 min in a refrigerated centrifuge. The supernatants were collected, aliquoted, and immediately frozen at −80°C.

Nuclear and cytoplasmic fractionation

Our nuclear-cytoplasmic fractionation technique was adapted from a previously described method (*104*). Cytoplasmic buffer stock (1×) was as follows: 10 mM Hepes, 10 mM KCl, and 0.1 mM EDTA (pH 7.9). Nuclear buffer stock (1×) was as follows: 20 mM Hepes, 0.42 M NaCl, and 0.1 mM EDTA (pH 7.9). Both buffers were stored at 4°C. The night before use, one tablet each of phosphatase inhibitor (PhosSTOP, Roche) and proteasome inhibitor (cOmplete, Roche) was added to a working volume of each buffer. On the day of lysate collection, T cells were harvested from the culture, washed with ice-cold PBS (Corning), and resuspended in the working stock of ice-cold cytoplasmic buffer. Samples were incubated on ice for 10 min. A final concentration of 0.1% NP-40 (Thermo Fisher Scientific) was added to each sample. Each sample was then incubated at room temperature for 5 min, followed by a 10-s maximum speed vortex and immediate centrifugation at 4000*g* for 90 s at 4°C. Supernatants were collected on ice, aliquoted, and frozen at −80°C for later use as the cytoplasmic fraction. The remaining nuclear pellets were washed twice with ice-cold cytoplasmic buffer and transferred to a fresh tube. They were then resuspended in ice-cold nuclear buffer and shaken at 4°C for 30 min at 1400 rpm. Samples were then centrifuged at 16,000*g* for 15 min at 4°C. Supernatants were collected, aliquoted on ice, and stored at −80°C to be used as nuclear fractions.

Western blotting analysis

Cell lysates were thawed on ice, and protein concentration was assessed by DC Protein Assay (Bio-Rad) according to the manufacturer's instructions. Equal quantities of protein were added to Laemmli buffer (Bio-Rad) containing 2-mercaptoethanol (Bio-Rad) and boiled at 95°C for 5 min. Protein was separated in NuPAGE gels using the Cell SureLock Mini-Cell (Invitrogen) and transferred to a methanol-activated PVDF-FL membrane (Millipore Sigma) in the Mini Trans-Blot Electrophoretic Transfer Cell (Bio-Rad) in 10% methanol NuPAGE transfer buffer (Thermo Fisher Scientific). After transfer, the membranes were incubated in methanol for 1 min, followed by a deionized water wash, and then incubated in tris-buffered saline (TBS) for 2 min before being blocked in TBS Odyssey blocking buffer (LI-COR) for 1 hour. Proteins were visualized with the primary antibodies against the following targets and incubated overnight at 4°C in TBS Odyssey blocking buffer (LI-COR) with 0.5% Tween 20 (Bio-Rad): PCNA (1:2000; PC10, Cell Signaling Technology), actin (1:1000; 8H10D10, Cell Signaling Technology), pZap-70 (1:1000; Tyr^{319}, 65E4, Cell Signaling Technology), Zap-70 (1:1000; L1E5, Cell Signaling Technology), pp65 (1:1000; Ser^{536}, 93H1, Cell Signaling Technology), p65 (1:1000; L8F6, Cell Signaling Technology), pp44/42 mitogen-activated protein kinase (MAPK) (ERK1/2) (1:2000; Tyr^{202}/Tyr^{204}, D13.14.4E, Cell Signaling Technology), p44/42 MAPK (ERK1/2) (1:2000; L34F12, Cell Signaling Technology), NIK (1:750; Cell Signaling Technology), pNF-κB2 p100 (1:1000; Ser^{866}/Ser^{870}, Cell Signaling Technology), NF-κB p52 (1:1000; Millipore Sigma), RelB (1:1000; D7D7W, Cell Signaling Technology), and Bim (1:1000; C34C5, Cell Signaling Technology). Each membrane was only incubated with one primary antibody from a single origin species (rabbit or mouse) at one time. The membranes were washed with TBS containing 0.1% Tween 20 and incubated with donkey anti-rabbit (1:15,000; IRDye 800CW, LI-COR), donkey anti-mouse (1:15,000; IRDye 680RD, LI-COR), or both secondary antibodies in TBS Odyssey blocking buffer (LI-COR) with 0.5% Tween 20 and 0.1% SDS (Thermo Fisher Scientific) for 40 min at room temperature. The membranes were then washed again with TBS containing 0.1% Tween 20, rinsed once in TBS, and then kept in TBS at 4°C until imaging. Membranes were imaged with an Odyssey CLx (LI-COR), and fluorescence was evaluated with Image Studio (LI-COR). When membranes were reused to visualize additional proteins, they were first reblocked in TBS Odyssey blocking buffer (LI-COR) for 1 hour at room temperature and then processed as described earlier.

Statistical analysis

Results are expressed as means ± SD. All Log_{FC} values are derived as follows: Log_2 of ((time of interest of experimental group: raw fluorescence of the protein of interest/raw fluorescence of relevant loading control)/(control time point of control group: raw fluorescence of protein of interest/raw fluorescence of relevant loading control)). Analysis of relative protein abundance in Fig. 5 (D and E) was determined by calculating the ratio of the fluorescence intensity of the stated protein sample to the fluorescence intensity of the same protein with the lowest abundance sample in the experiment. Statistical comparisons were made as noted in the figure legends, with the factors of two-way analysis of variance (ANOVA) analyses being CAR and time using Prism (GraphPad).

SUPPLEMENTARY MATERIALS

stke.sciencemag.org/cgi/content/full/13/625/eaay8248/DC1

Fig. S1. The ncNF-κB pathway.

Fig. S2. CAR expression on T cells from three donors expanded by irradiated Nalm6 cells.

Fig. S3. CAR expression on T cells from three donors expanded by anti-CD19 beads.

Fig. S4. CAR expression on T cells from three donors activated by anti-CD19 beads for signaling assays.

Fig. S5. Anti-CD19 BBζ CAR activation induces T cell signaling.

Fig. S6. Additional representative Western blotting analysis of nuclear and cytoplasmic fractions to compare anti-CD19 CAR signaling.

Fig. S7. Anti-mesothelin BBζ CAR also drives ncNF-κB signaling.
Fig. S8. Dual-transduced T cell production scheme, day 0 CAR, and mCherry expression.
Fig. S9. Western blotting analysis of nuclear and cytoplasmic fractions to compare control and dnNIK-expressing anti-CD19 BBζ T cells.
Fig. S10. dnNIK does not affect PCNA abundance in CAR T cells.
Fig. S11. Bim_{EL} abundance in anti-CD19 CAR T cells.
Fig. S12. ERK1/2 phosphorylation in control and dnNIK-expressing BBζ CAR T cells.
Fig. S13. FOXO3a abundance and phosphorylation in control and dnNIK-expressing BBζ CAR T cells.
Fig. S14. CAR constructs.
Fig. S15. Representative gating strategy to quantify cell death by flow cytometry and assess the elimination of $CD19^+$ Nalm6 cells.

View/request a protocol for this paper from *Bio-protocol*.

REFERENCES AND NOTES

1. S. Feins, W. Kong, E. F. Williams, M. C. Milone, J. A. Fraietta, An introduction to chimeric antigen receptor (CAR) T-cell immunotherapy for human cancer. *Am. J. Hematol.* **94**, S3–S9 (2019).
2. K. T. Mueller, E. Waldron, S. A. Grupp, J. E. Levine, T. W. Laetsch, M. A. Pulsipher, M. W. Boyer, K. J. August, J. Hamilton, R. Awasthi, A. M. Stein, D. Sickert, A. Chakraborty, B. L. Levine, C. H. June, L. Tomassian, S. S. Shah, M. Leung, T. Taran, P. A. Wood, S. L. Maude, Clinical pharmacology of tisagenlecleucel in B-cell acute lymphoblastic leukemia. *Clin. Cancer Res.* **24**, 6175–6184 (2018).
3. E. J. Orlando, X. Han, C. Tribouley, P. A. Wood, R. J. Leary, M. Riester, J. E. Levine, M. Qayed, S. A. Grupp, M. Boyer, B. De Moerloose, E. R. Nemecek, H. Bittencourt, H. Hiramatsu, J. Buechner, S. M. Davies, M. R. Verneris, K. Nguyen, J. L. Brogdon, H. Bitter, M. Morrissey, P. Pierog, S. Pantano, J. A. Engelman, W. Winckler, Genetic mechanisms of target antigen loss in CAR19 therapy of acute lymphoblastic leukemia. *Nat. Med.* **24**, 1504–1506 (2018).
4. K. T. Mueller, S. L. Maude, D. L. Porter, N. Frey, P. Wood, X. Han, E. Waldron, A. Chakraborty, R. Awasthi, B. L. Levine, J. J. Melenhorst, S. A. Grupp, C. H. June, S. F. Lacey, Cellular kinetics of CTL019 in relapsed/refractory B-cell acute lymphoblastic leukemia and chronic lymphocytic leukemia. *Blood* **130**, 2317–2325 (2017).
5. C. J. Turtle, L.-A. Hanafi, C. Berger, T. A. Gooley, S. Cherian, M. Hudecek, D. Sommermeyer, K. Melville, B. Pender, T. M. Budiarto, E. Robinson, N. N. Steevens, C. Chaney, L. Soma, X. Chen, C. Yeung, B. Wood, D. Li, J. Cao, S. Heimfeld, M. C. Jensen, S. R. Riddell, D. G. Maloney, CD19 CAR-T cells of defined $CD4^+$: $CD8^+$composition in adult B cell ALL patients. *J. Clin. Invest.* **126**, 2123–2138 (2016).
6. S. J. C. van der Stegen, M. Hamieh, M. Sadelain, The pharmacology of second-generation chimeric antigen receptors. *Nat. Rev. Drug Discov.* **14**, 499–509 (2015).
7. S. S. Neelapu, F. L. Locke, N. L. Bartlett, L. J. Lekakis, D. B. Miklos, C. A. Jacobson, I. Braunschweig, O. O. Oluwole, T. Siddiqi, Y. Lin, J. M. Timmerman, P. J. Stiff, J. W. Friedberg, I. W. Flinn, A. Goy, B. T. Hill, M. R. Smith, A. Deol, U. Farooq, P. McSweeney, J. Munoz, I. Avivi, J. E. Castro, J. R. Westin, J. C. Chavez, A. Ghobadi, K. V. Komanduri, R. Levy, E. D. Jacobsen, T. E. Witzig, P. Reagan, A. Bot, J. Rossi, L. Navale, Y. Jiang, J. Aycock, M. Elias, D. Chang, J. Wiezorek, W. Y. Go, Axicabtagene ciloleucel CAR T-cell therapy in refractory large B-cell lymphoma. *N. Engl. J. Med.* **377**, 2531–2544 (2017).
8. S. L. Maude, T. W. Laetsch, J. Buechner, S. Rives, M. Boyer, H. Bittencourt, P. Bader, M. R. Verneris, H. E. Stefanski, G. D. Myers, M. Qayed, B. De Moerloose, H. Hiramatsu, K. Schlis, K. L. Davis, P. L. Martin, E. R. Nemecek, G. A. Yanik, C. Peters, A. Baruchel, N. Boissel, F. Mechinaud, A. Balduzzi, J. Krueger, C. H. June, B. L. Levine, P. Wood, T. Taran, M. Leung, K. T. Mueller, Y. Zhang, K. Sen, D. Lebwohl, M. A. Pulsipher, S. A. Grupp, Tisagenlecleucel in children and young adults with B-cell lymphoblastic leukemia. *N. Engl. J. Med.* **378**, 439–448 (2018).
9. R. Weinkove, P. George, N. Dasyam, A. D. McLellan, Selecting costimulatory domains for chimeric antigen receptors: Functional and clinical considerations. *Clin. Transl. Immunol.* **8**, e1049 (2019).
10. A. H. Long, W. M. Haso, J. F. Shern, K. M. Wanhainen, M. Murgai, M. Ingaramo, J. P. Smith, A. J. Walker, M. E. Kohler, V. R. Venkateshwara, R. N. Kaplan, G. H. Patterson, T. J. Fry, R. J. Orentas, C. L. Mackall, 4-1BB costimulation ameliorates T cell exhaustion induced by tonic signaling of chimeric antigen receptors. *Nat. Med.* **21**, 581–590 (2015).
11. M. J. Frigault, J. Lee, M. C. Basil, C. Carpenito, S. Motohashi, J. Scholler, O. U. Kawalekar, S. Guedan, S. E. McGettigan, A. D. Posey, S. Ang, L. J. N. Cooper, J. M. Platt, F. B. Johnson, C. M. Paulos, Y. Zhao, M. Kalos, M. C. Milone, C. H. June, Identification of chimeric antigen receptors that mediate constitutive or inducible proliferation of T cells. *Cancer Immunol. Res.* **3**, 356–367 (2015).
12. A. I. Salter, R. G. Ivey, J. J. Kennedy, V. Voillet, A. Rajan, E. J. Alderman, U. J. Voytovich, C. Lin, D. Sommermeyer, L. Liu, J. R. Whiteaker, R. Gottardo, A. G. Paulovich, S. R. Riddell, Phosphoproteomic analysis of chimeric antigen receptor signaling reveals kinetic and quantitative differences that affect cell function. *Sci. Signal.* **11**, eaat6753 (2018).
13. J. Feucht, J. Sun, J. Eyquem, Y.-J. Ho, Z. Zhao, J. Leibold, A. Dobrin, A. Cabriolu, M. Hamieh, M. Sadelain, Calibration of CAR activation potential directs alternative T cell fates and therapeutic potency. *Nat. Med.* **25**, 82–88 (2019).
14. Z. Zhao, M. Condomines, S. J. C. van der Stegen, F. Perna, C. C. Kloss, G. Gunset, J. Plotkin, M. Sadelain, Structural design of engineered costimulation determines tumor rejection kinetics and persistence of CAR T cells. *Cancer Cell* **28**, 415–428 (2015).
15. E. Drent, R. Poels, R. Ruiter, N. W. C. J. van de Donk, S. Zweegman, H. Yuan, J. de Bruijn, M. Sadelain, H. M. Lokhorst, R. Groen, T. Mutis, M. Themeli, Combined CD28 and 4-1BB costimulation potentiates affinity-tuned chimeric antigen receptor-engineered T cells. *Clin. Cancer Res.* **25**, 4014–4025 (2019).
16. H.-W. Lee, S.-J. Park, B. K. Choi, H. H. Kim, K.-O. Nam, B. S. Kwon, 4-1BB promotes the survival of CD8+ T lymphocytes by increasing expression of Bcl-xL and Bfl-1. *J. Immunol.* **169**, 4882–4888 (2002).
17. W. W. Shuford, K. Klussman, D. D. Tritchler, D. T. Loo, J. Chalupny, A. W. Siadak, T. J. Brown, J. Emswiler, H. Raecho, C. P. Larsen, T. C. Pearson, J. A. Ledbetter, A. Aruffo, R. S. Mittler, 4-1BB costimulatory signals preferentially induce CD8+ T cell proliferation and lead to the amplification in vivo of cytotoxic T cell responses. *J. Exp. Med.* **186**, 47–55 (1997).
18. M. L. Giardino Torchia, I. Munitic, E. Castro, J. Herz, D. B. McGavern, J. D. Ashwell, c-IAP ubiquitin protein ligase activity is required for 4-1BB signaling and $CD8^+$ memory T-cell survival. *Eur. J. Immunol.* **45**, 2672–2682 (2015).
19. E. M. Bertram, P. Lau, T. H. Watts, Temporal segregation of 4-1BB versus CD28-mediated costimulation: 4-1BB ligand influences T cell numbers late in the primary response and regulates the size of the T cell memory response following influenza infection. *J. Immunol.* **168**, 3777–3785 (2002).
20. J. C. Hurtado, Y. J. Kim, B. S. Kwon, Signals through 4-1BB are costimulatory to previously activated splenic T cells and inhibit activation-induced cell death. *J. Immunol.* **158**, 2600–2609 (1997).
21. J. Hendriks, Y. Xiao, J. W. A. Rossen, K. F. van der Sluijs, K. Sugamura, N. Ishii, J. Borst, During viral infection of the respiratory tract, CD27, 4-1BB, and OX40 collectively determine formation of $CD8^+$ memory T cells and their capacity for secondary expansion. *J. Immunol.* **175**, 1665–1676 (2005).
22. L. M. Snell, G. H. Y. Lin, A. J. McPherson, T. J. Moraes, T. H. Watts, T-cell intrinsic effects of GITR and 4-1BB during viral infection and cancer immunotherapy. *Immunol. Rev.* **244**, 197–217 (2011).
23. Y. Li, C. E. Sedwick, J. Hu, A. Altman, Role for protein kinase Cθ (PKCθ) in TCR/CD28-mediated signaling through the canonical but not the non-canonical pathway for NF-κB activation. *J. Biol. Chem.* **280**, 1217–1223 (2005).
24. A. J. McPherson, L. M. Snell, T. W. Mak, T. H. Watts, Opposing roles for TRAF1 in the alternative versus classical NF-κB pathway in T cells. *J. Biol. Chem.* **287**, 23010–23019 (2012).
25. X. Xiao, X. Shi, Y. Fan, C. Wu, X. Zhang, L. Minze, W. Liu, R. M. Ghobrial, P. Lan, X. C. Li, The costimulatory receptor OX40 inhibits interleukin-17 expression through activation of repressive chromatin remodeling pathways. *Immunity* **44**, 1271–1283 (2016).
26. P. Ramakrishnan, W. Wang, D. Wallach, Receptor-specific signaling for both the alternative and the canonical NF-kappaB activation pathways by NF-κB-inducing kinase. *Immunity* **21**, 477–489 (2004).
27. L. P. Kane, J. Lin, A. Weiss, It's all Rel-ative: NF-κB and CD28 costimulation of T-cell activation. *Trends Immunol.* **23**, 413–420 (2002).
28. Z. Sun, C. W. Arendt, W. Ellmeier, E. M. Schaeffer, M. J. Sunshine, L. Gandhi, J. Annes, D. Petrzilka, A. Kupfer, P. L. Schwartzberg, D. R. Littman, PKC-theta is required for TCR-induced NF-kappaB activation in mature but not immature T lymphocytes. *Nature* **404**, 402–407 (2000).
29. G. Schimmack, A. C. Eitelhuber, M. Vincendeau, K. Demski, H. Shinohara, T. Kurosaki, D. Krappmann, AIP augments CARMA1-BCL10-MALT1 complex formation to facilitate NF-κB signaling upon T cell activation. *Cell Commun. Signal* **12**, 49 (2014).
30. R. Shinkura, K. Kitada, F. Matsuda, K. Tashiro, K. Ikuta, M. Suzuki, K. Kogishi, T. Serikawa, T. Honjo, Alymphoplasia is caused by a point mutation in the mouse gene encoding Nf-κb-inducing kinase. *Nat. Genet.* **22**, 74–77 (1999).
31. E. Claudio, K. Brown, S. Park, H. Wang, U. Siebenlist, BAFF-induced NEMO-independent processing of NF-κ B2 in maturing B cells. *Nat. Immunol.* **3**, 958–965 (2002).
32. K. L. Willmann, S. Klaver, F. Doğu, E. Santos-Valente, W. Garncarz, I. Bilic, E. Mace, E. Salzer, C. D. Conde, H. Sic, P. Májek, P. P. Banerjee, G. I. Vladimer, S. Haskoloğlu, M. G. Bolkent, A. Küpesiz, A. Condino-Neto, J. Colinge, G. Superti-Furga, W. F. Pickl, M. C. van Zelm, H. Eibel, J. S. Orange, A. Ikincioğulları, K. Boztug, Biallelic loss-of-function mutation in NIK causes a primary immunodeficiency with multifaceted aberrant lymphoid immunity. *Nat. Commun.* **5**, 5360 (2014).
33. A. G. Eliopoulos, J. H. Caamano, J. Flavell, G. M. Reynolds, P. G. Murray, J.-L. Poyet, L. S. Young, Epstein-Barr virus-encoded latent infection membrane protein 1 regulates the processing of p100 NF-κB2 to p52 via an IKKγ/NEMO-independent signalling pathway. *Oncogene* **22**, 7557–7569 (2003).
34. F. Cormier, H. Monjanel, C. Fabre, K. Billot, E. Sapharikas, F. Chereau, D. Bordereaux, T. J. Molina, H. Avet-Loiseau, V. Baud, L. Bendall, Frequent engagement of RelB activation is critical for cell survival in multiple myeloma. *PLOS ONE* **8**, e59127 (2013).
35. S. D. Vallabhapurapu, S. K. Noothi, D. A. Pullum, C. H. Lawrie, R. Pallapati, V. Potluri, C. Kuntzen, S. Khan, D. R. Plas, R. Z. Orlowski, M. Chesi, W. M. Kuehl, P. L. Bergsagel,

M. Karin, S. Vallabhapurapu, Transcriptional repression by the HDAC4-RelB-p52 complex regulates multiple myeloma survival and growth. *Nat. Commun.* **6**, 8428 (2015).
36. S. M. Ranuncolo, S. Pittaluga, M. O. Evbuomwan, E. S. Jaffe, B. A. Lewis, Hodgkin lymphoma requires stabilized NIK and constitutive RelB expression for survival. *Blood* **120**, 3756–3763 (2012).
37. C. E. Wharry, K. M. Haines, R. G. Carroll, M. J. May, Constitutive non-canonical NFκB signaling in pancreatic cancer cells. *Cancer Biol. Ther.* **8**, 1567–1576 (2009).
38. S.-C. Sun, The non-canonical NF-κB pathway in immunity and inflammation. *Nat. Rev. Immunol.* **17**, 545–558 (2017).
39. Y. Li, H. Wang, X. Zhou, X. Xie, X. Chen, Z. Jie, Q. Zou, H. Hu, L. Zhu, X. Cheng, H. D. Brightbill, L. C. Wu, L. Wang, S.-C. Sun, Cell intrinsic role of NF-κB-inducing kinase in regulating T cell-mediated immune and autoimmune responses. *Sci. Rep.* **6**, 22115 (2016).
40. A. M. Rowe, S. E. Murray, H.-P. Raué, Y. Koguchi, M. K. Slifka, D. C. Parker, A cell-intrinsic requirement for NF-κB-inducing kinase in CD4 and CD8 T cell memory. *J. Immunol.* **191**, 3663–3672 (2013).
41. M. C. Milone, J. D. Fish, C. Carpenito, R. G. Carroll, G. K. Binder, D. Teachey, M. Samanta, M. Lakhal, B. Gloss, G. Danet-Desnoyers, D. Campana, J. L. Riley, S. A. Grupp, C. H. June, Chimeric receptors containing CD137 signal transduction domains mediate enhanced survival of T cells and increased antileukemic efficacy in vivo. *Mol. Ther.* **17**, 1453–1464 (2009).
42. W. Li, D. Fan, M. Yang, Y. Yan, R. Shi, J. Cheng, Z. Li, M. Zhang, J. Wang, D. Xiong, Cytosine arabinoside promotes cytotoxic effect of T cells on leukemia cells mediated by bispecific antibody. *Hum. Gene Ther.* **24**, 751–760 (2013).
43. O. U. Kawalekar, R. S. O'Connor, J. A. Fraietta, L. Guo, S. E. McGettigan, A. D. Posey, P. R. Patel, S. Guedan, J. Scholler, B. Keith, N. Snyder, I. Blair, M. C. Milone, C. H. June, Distinct signaling of coreceptors regulates specific metabolism pathways and impacts memory development in CAR T cells. *Immunity* **44**, 380–390 (2016).
44. M. C. Ramello, I. Benzaïd, B. M. Kuenzi, M. Lienlaf-Moreno, W. M. Kandell, D. N. Santiago, M. Pabón-Saldaña, L. Darville, B. Fang, U. Rix, S. Yoder, A. Berglund, J. M. Koomen, E. B. Haura, D. Abate-Daga, An immunoproteomic approach to characterize the CAR interactome and signalosome. *Sci. Signal.* **12**, eaap9777 (2019).
45. K. V. Salojin, J. Zhang, T. L. Delovitch, TCR and CD28 are coupled via ZAP-70 to the activation of the Vav/Rac-1-/PAK-1/p38 MAPK signaling pathway. *J. Immunol.* **163**, 844–853 (1999).
46. W. N. D'Souza, C.-F. Chang, A. M. Fischer, M. Li, S. M. Hedrick, The Erk2 MAPK regulates CD8 T cell proliferation and survival. *J. Immunol.* **181**, 7617–7629 (2008).
47. X. Liu, C. T. Berry, G. Ruthel, J. J. Madara, K. MacGillivray, C. M. Gray, L. A. Madge, K. A. McCorkell, D. P. Beiting, U. Hershberg, M. J. May, B. D. Freedman, T cell receptor-induced nuclear factor κB (NF-κB) signaling and transcriptional activation are regulated by STIM1- and Orai1-mediated calcium entry. *J. Biol. Chem.* **291**, 8440–8452 (2016).
48. C. Remouchamps, E. Dejardin, Methods to assess the activation of the alternative (noncanonical) NF-κB pathway by non-death TNF receptors. *Methods Mol. Biol.* **1280**, 103–119 (2015).
49. A. R. Sanchez-Paulete, S. Labiano, M. E. Rodriguez-Ruiz, A. Azpilikueta, I. Etxeberria, E. Bolaños, V. Lang, M. Rodriguez, M. A. Aznar, M. Jure-Kunkel, I. Melero, Deciphering CD137 (4-1BB) signaling in T-cell costimulation for translation into successful cancer immunotherapy. *Eur. J. Immunol.* **46**, 513–522 (2016).
50. S.-C. Sun, The noncanonical NF-κB pathway. *Immunol. Rev.* **246**, 125–140 (2012).
51. G. Xiao, E. W. Harhaj, S. C. Sun, NF-κB-inducing kinase regulates the processing of NF-kappaB2 p100. *Mol. Cell* **7**, 401–409 (2001).
52. Z. Wang, B. Zhang, L. Yang, J. Ding, H.-F. Ding, Constitutive production of NF-κB2 p52 is not tumorigenic but predisposes mice to inflammatory autoimmune disease by repressing Bim expression. *J. Biol. Chem.* **283**, 10698–10706 (2008).
53. L. Sabbagh, G. Pulle, Y. Liu, E. N. Tsitsikov, T. H. Watts, ERK-dependent Bim modulation downstream of the 4-1BB-TRAF1 signaling axis is a critical mediator of CD8 T cell survival in vivo. *J. Immunol.* **180**, 8093–8101 (2008).
54. F. Luciano, A. Jacquel, P. Colosetti, M. Herrant, S. Cagnol, G. Pages, P. Auberger, Phosphorylation of Bim-EL by Erk1/2 on serine 69 promotes its degradation via the proteasome pathway and regulates its proapoptotic function. *Oncogene* **22**, 6785–6793 (2003).
55. L. A. O'Reilly, E. A. Kruse, H. Puthalakath, P. N. Kelly, T. Kaufmann, D. C. S. Huang, A. Strasser, MEK/ERK-mediated phosphorylation of Bim is required to ensure survival of T and B lymphocytes during mitogenic stimulation. *J. Immunol.* **183**, 261–269 (2009).
56. C. Riou, B. Yassine-Diab, J. Van Grevenynghe, R. Somogyi, L. D. Greller, D. Gagnon, S. Gimmig, P. Wilkinson, Y. Shi, M. J. Cameron, R. Campos-Gonzalez, R. S. Balderas, D. Kelvin, R.-P. Sekaly, E. K. Haddad, Convergence of TCR and cytokine signaling leads to FOXO3a phosphorylation and drives the survival of $CD4^+$ central memory T cells. *J. Exp. Med.* **204**, 79–91 (2007).
57. A. Sunters, S. Fernández de Mattos, M. Stahl, J. J. Brosens, G. Zoumpoulidou, C. A. Saunders, P. J. Coffer, R. H. Medema, R. C. Coombes, E. W.-F. Lam, FoxO3a transcriptional regulation of Bim controls apoptosis in paclitaxel-treated breast cancer cell lines. *J. Biol. Chem.* **278**, 49795–49805 (2003).
58. B. Marinari, A. Costanzo, V. Marzano, E. Piccolella, L. Tuosto, CD28 delivers a unique signal leading to the selective recruitment of RelA and p52 NF-κB subunits on IL-8 and Bcl-xL gene promoters. *Proc. Natl. Acad. Sci. U.S.A.* **101**, 6098–6103 (2004).
59. A. Ajina, J. Maher, Strategies to address chimeric antigen receptor tonic signaling. *Mol. Cancer Ther.* **17**, 1795–1815 (2018).
60. G. Li, J. C. Boucher, H. Kotani, K. Park, Y. Zhang, B. Shrestha, X. Wang, L. Guan, N. Beatty, D. Abate-Daga, M. L. Davila, 4-1BB enhancement of CAR T function requires NF-κB and TRAFs. *JCI Insight* **3**, 1999 (2018).
61. P. M. Snow, C. Terhorst, The T8 antigen is a multimeric complex of two distinct subunits on human thymocytes but consists of homomultimeric forms on peripheral blood T lymphocytes. *J. Biol. Chem.* **258**, 14675–14681 (1983).
62. D. T. Harris, D. M. Kranz, Adoptive T cell therapies: A comparison of T cell receptors and chimeric antigen receptors. *Trends Pharmacol. Sci.* **37**, 220–230 (2015).
63. A. Bitra, T. Doukov, M. Croft, D. M. Zajonc, Crystal structures of the human 4-1BB receptor bound to its ligand 4-1BBL reveal covalent receptor dimerization as a potential signaling amplifier. *J. Biol. Chem.* **293**, 1317–1329 (2018).
64. E.-Y. Won, K. Cha, J.-S. Byun, D.-U. Kim, S. Shin, B. Ahn, Y. H. Kim, A. J. Rice, T. Walz, B. S. Kwon, H.-S. Cho, The structure of the trimer of human 4-1BB ligand is unique among members of the tumor necrosis factor superfamily. *J. Biol. Chem.* **285**, 9202–9210 (2010).
65. R. N. Gilbreth, V. Y. Oganesyan, H. Amdouni, S. Novarra, L. Grinberg, A. Barnes, M. Baca, Crystal structure of the human 4-1BB/4-1BBL complex. *J. Biol. Chem.* **293**, 9880–9891 (2018).
66. C. Zheng, V. Kabaleeswaran, Y. Wang, G. Cheng, H. Wu, Crystal structures of the TRAF2: cIAP2 and the TRAF1: TRAF2: cIAP2 complexes: Affinity, specificity, and regulation. *Mol. Cell* **38**, 101–113 (2010).
67. J. M. Zapata, G. Perez-Chacon, P. Carr-Baena, I. Martinez-Forero, A. Azpilikueta, I. Otano, I. Melero, CD137 (4-1BB) signalosome: Complexity is a matter of TRAFs. *Front. Immunol.* **9**, 2618 (2018).
68. W. Zheng, C. E. O'Hear, R. Alli, J. H. Basham, H. A. Abdelsamed, L. E. Palmer, L. L. Jones, B. Youngblood, T. L. Geiger, PI3K orchestration of the in vivo persistence of chimeric antigen receptor-modified T cells. *Leukemia* **32**, 1157–1167 (2018).
69. E. Wang, L.-C. Wang, C.-Y. Tsai, V. Bhoj, Z. Gershenson, E. Moon, K. Newick, J. Sun, A. Lo, T. Baradet, M. D. Feldman, D. Barrett, E. Puré, S. Albelda, M. C. Milone, Generation of potent T-cell immunotherapy for cancer using DAP12-based, multichain, chimeric immunoreceptors. *Cancer Immunol. Res.* **3**, 815–826 (2015).
70. Y. Li, Q.-L. Zhou, W. Sun, P. Chandrasekharan, H. S. Cheng, Z. Ying, M. Lakshmanan, A. Raju, D. G. Tenen, S.-Y. Cheng, K.-H. Chuang, J. Li, S. Prabhakar, M. Li, V. Tergaonkar, Non-canonical NF-κB signalling and ETS1/2 cooperatively drive C250T mutant TERT promoter activation. *Nat. Cell Biol.* **17**, 1327–1338 (2015).
71. C. D. House, V. Grajales, M. Ozaki, E. Jordan, H. Wubneh, D. C. Kimble, J. M. James, M. K. Kim, C. M. Annunziata, IKKε cooperates with either MEK or non-canonical NF-kB driving growth of triple-negative breast cancer cells in different contexts. *BMC Cancer* **18**, 595 (2018).
72. M. Shinzawa, H. Konno, J. Qin, N. Akiyama, M. Miyauchi, H. Ohashi, E. Miyamoto-Sato, H. Yanagawa, T. Akiyama, J.-i. Inoue, Catalytic subunits of the phosphatase calcineurin interact with NF-κB-inducing kinase (NIK) and attenuate NIK-dependent gene expression. *Sci. Rep.* **5**, 10758 (2015).
73. Z. Liu, K. B. Mar, N. W. Hanners, S. S. Perelman, M. Kanchwala, C. Xing, J. W. Schoggins, N. M. Alto, A NIK-SIX signalling axis controls inflammation by targeted silencing of non-canonical NF-κB. *Nature* **22**, 249–253 (2019).
74. T. Mukherjee, B. Chatterjee, A. Dhar, S. S. Bais, M. Chawla, P. Roy, A. George, V. Bal, S. Rath, S. Basak, A TNF-p100 pathway subverts noncanonical NF-κB signaling in inflamed secondary lymphoid organs. *EMBO J.* , 3501–3516 (2017).
75. H. Liu, M. Rhodes, D. L. Wiest, D. A. Vignali, On the dynamics of TCR:CD3 complex cell surface expression and downmodulation. *Immunity* **13**, 665–675 (2000).
76. A. J. Walker, R. G. Majzner, L. Zhang, K. Wanhainen, A. H. Long, S. M. Nguyen, P. Lopomo, M. Vigny, T. J. Fry, R. J. Orentas, C. L. Mackall, Tumor antigen and receptor densities regulate efficacy of a chimeric antigen receptor targeting anaplastic lymphoma kinase. *Mol. Ther.* **25**, 2189–2201 (2017).
77. P. Soroosh, S. Ine, K. Sugamura, N. Ishii, OX40-OX40 ligand interaction through T cell-T cell contact contributes to CD4 T cell longevity. *J. Immunol.* **176**, 5975–5987 (2006).
78. K. Kondo, K. Okuma, R. Tanaka, L. F. Zhang, A. Kodama, Y. Takahashi, N. Yamamoto, A. A. Ansari, Y. Tanaka, Requirements for the functional expression of OX40 ligand on human activated $CD4^+$ and $CD8^+$ T cells. *Hum. Immunol.* **68**, 563–571 (2007).
79. S. E. Murray, F. Polesso, A. M. Rowe, S. Basak, Y. Koguchi, K. G. Toren, A. Hoffmann, D. C. Parker, NF-κB–inducing kinase plays an essential T cell–intrinsic role in graft-versus-host disease and lethal autoimmunity in mice. *J. Clin. Invest.* **121**, 4775–4786 (2011).
80. A. A. Hombach, H. Abken, Costimulation by chimeric antigen receptors revisited the T cell antitumor response benefits from combined CD28-OX40 signalling. *Int. J. Cancer* **129**, 2935–2944 (2011).

81. J. Michie, P. A. Beavis, A. J. Freeman, S. J. Vervoort, K. M. Ramsbottom, V. Narasimhan, E. J. Lelliott, N. Lalaoui, R. G. Ramsay, R. W. Johnstone, J. Silke, P. K. Darcy, I. Voskoboinik, C. J. Kearney, J. Oliaro, Antagonism of IAPs enhances CAR T-cell efficacy. *Cancer Immunol. Res.* **7**, 183–192 (2019).
82. A. Tchoghandjian, C. Jennewein, I. Eckhardt, K. Rajalingam, S. Fulda, Identification of non-canonical NF-κB signaling as a critical mediator of Smac mimetic-stimulated migration and invasion of glioblastoma cells. *Cell Death Dis.* **4**, e564 (2013).
83. M. Dougan, S. Dougan, J. Slisz, B. Firestone, M. Vanneman, D. Draganov, G. Goyal, W. Li, D. Neuberg, R. Blumberg, N. Hacohen, D. Porter, L. Zawel, G. Dranoff, IAP inhibitors enhance co-stimulation to promote tumor immunity. *J. Exp. Med.* **207**, 2195–2206 (2010).
84. M. F. Krummel, W. R. Heath, J. Allison, Differential coupling of second signals for cytotoxicity and proliferation in $CD8^+$ T cell effectors: Amplification of the lytic potential by B7. *J. Immunol.* **163**, 2999–3006 (1999).
85. L. A. Johnson, R. A. Morgan, M. E. Dudley, L. Cassard, J. C. Yang, M. S. Hughes, U. S. Kammula, R. E. Royal, R. M. Sherry, J. R. Wunderlich, C.-C. R. Lee, N. P. Restifo, S. L. Schwarz, A. P. Cogdill, R. J. Bishop, H. Kim, C. C. Brewer, S. F. Rudy, C. VanWaes, J. L. Davis, A. Mathur, R. T. Ripley, D. A. Nathan, C. M. Laurencot, S. A. Rosenberg, Gene therapy with human and mouse T-cell receptors mediates cancer regression and targets normal tissues expressing cognate antigen. *Blood* **114**, 535–546 (2009).
86. S. T. Beug, C. E. Beauregard, C. Healy, T. Sanda, M. St-Jean, J. Chabot, D. E. Walker, A. Mohan, N. Earl, X. Lun, D. L. Senger, S. M. Robbins, P. Staeheli, P. A. Forsyth, T. Alain, E. C. LaCasse, R. G. Korneluk, Smac mimetics synergize with immune checkpoint inhibitors to promote tumour immunity against glioblastoma. *Nat. Commun.* **8**, 14278 (2017).
87. S. Wojciechowski, M. B. Jordan, Y. Zhu, J. White, A. J. Zajac, D. A. Hildeman, Bim mediates apoptosis of $CD127^{lo}$ effector T cells and limits T cell memory. *Eur. J. Immunol.* **36**, 1694–1706 (2006).
88. D. A. Hildeman, Y. Zhu, T. C. Mitchell, P. Bouillet, A. Strasser, J. Kappler, P. Marrack, Activated T cell death in vivo mediated by proapoptotic bcl-2 family member bim. *Immunity* **16**, 759–767 (2002).
89. P. Bouillet, J. F. Purton, D. I. Godfrey, L.-C. Zhang, L. Coultas, H. Puthalakath, M. Pellegrini, S. Cory, J. M. Adams, A. Strasser, BH3-only Bcl-2 family member Bim is required for apoptosis of autoreactive thymocytes. *Nature* **415**, 922–926 (2002).
90. F. Masson, F. Kupresanin, A. Mount, A. Strasser, G. T. Belz, Bid and Bim collaborate during induction of T cell death in persistent infection. *J. Immunol.* **186**, 4059–4066 (2011).
91. E. Sandalova, C.-H. Wei, M. G. Masucci, V. Levitsky, Regulation of expression of Bcl-2 protein family member Bim by T cell receptor triggering. *Proc. Natl. Acad. Sci. U.S.A.* **101**, 3011–3016 (2004).
92. A. L. Snow, J. B. Oliveira, L. Zheng, J. K. Dale, T. A. Fleisher, M. J. Lenardo, Critical role for BIM in T cell receptor restimulation-induced death. *Biol. Direct* **3**, 34 (2008).
93. R. Ley, K. Hadfield, E. Howes, S. J. Cook, Identification of a DEF-type docking domain for extracellular signal-regulated kinases 1/2 that directs phosphorylation and turnover of the BH3-only protein BimEL. *J. Biol. Chem.* **280**, 17657–17663 (2005).
94. L. O'Connor, A. Strasser, L. A. O'Reilly, G. Hausmann, J. M. Adams, S. Cory, D. C. Huang, Bim: A novel member of the Bcl-2 family that promotes apoptosis. *EMBO J.* **17**, 384–395 (1998).
95. C. Clybouw, D. Merino, T. Nebl, F. Masson, M. Robati, L. O'Reilly, A. Hübner, R. J. Davis, A. Strasser, P. Bouillet, Alternative splicing of Bim and Erk-mediated Bim(EL) phosphorylation are dispensable for hematopoietic homeostasis in vivo. *Cell Death Differ.* **19**, 1060–1068 (2012).
96. C. Carpenito, M. C. Milone, R. Hassan, J. C. Simonet, M. Lakhal, M. M. Suhoski, A. Varela-Rohena, K. M. Haines, D. F. Heitjan, S. M. Albelda, R. G. Carroll, J. L. Riley, I. Pastan, C. H. June, Control of large, established tumor xenografts with genetically retargeted human T cells containing CD28 and CD137 domains. *Proc. Natl. Acad. Sci. U.S.A.* **106**, 3360–3365 (2009).
97. S. Guedan, A. D. Posey, C. Shaw, A. Wing, T. Da, P. R. Patel, S. E. McGettigan, V. Casado-Medrano, O. U. Kawalekar, M. Uribe-Herranz, D. Song, J. J. Melenhorst, S. F. Lacey, J. Scholler, B. Keith, R. M. Young, C. H. June, Enhancing CAR T cell persistence through ICOS and 4-1BB costimulation. *JCI Insight* **3**, e96976 (2018).
98. D.-G. Song, Q. Ye, C. Carpenito, M. Poussin, L.-P. Wang, C. Ji, M. Figini, C. H. June, G. Coukos, D. J. Powell, In vivo persistence, tumor localization, and antitumor activity of CAR-engineered T cells is enhanced by costimulatory signaling through CD137 (4-1BB). *Cancer Res.* **71**, 4617–4627 (2011).
99. S. J. Priceman, E. A. Gerdts, D. Tilakawardane, K. T. Kennewick, J. P. Murad, A. K. Park, B. Jeang, Y. Yamaguchi, X. Yang, R. Urak, L. Weng, W.-C. Chang, S. Wright, S. Pal, R. E. Reiter, A. M. Wu, C. E. Brown, S. J. Forman, Co-stimulatory signaling determines tumor antigen sensitivity and persistence of CAR T cells targeting PSCA+ metastatic prostate cancer. *Oncoimmunology* **7**, e1380764 (2018).
100. A. Paul, J. Edwards, C. Pepper, S. Mackay, Inhibitory-κB Kinase (IKK) α and nuclear factor-κB (NFκB)-inducing kinase (NIK) as anti-cancer drug targets. *Cell* **7**, 176 (2018).
101. J. Yu, X. Zhou, M. Nakaya, W. Jin, X. Cheng, S.-C. Sun, T cell-intrinsic function of the noncanonical NF-κB pathway in the regulation of GM-CSF expression and experimental autoimmune encephalomyelitis pathogenesis. *J. Immunol.* **193**, 422–430 (2014).
102. R. M. Sterner, R. Sakemura, M. J. Cox, N. Yang, R. H. Khadka, C. L. Forsman, M. J. Hansen, F. Jin, K. Ayasoufi, M. Hefazi, K. J. Schick, D. K. Walters, O. Ahmed, D. Chappell, T. Sahmoud, C. Durrant, W. K. Nevala, M. M. Patnaik, L. R. Pease, K. E. Hedin, N. E. Kay, A. J. Johnson, S. S. Kenderian, GM-CSF inhibition reduces cytokine release syndrome and neuroinflammation but enhances CAR-T cell function in xenografts. *Blood* **133**, 697–709 (2019).
103. M. Sachdeva, P. Duchateau, S. Depil, L. Poirot, J. Valton, Granulocyte-macrophage colony-stimulating factor inactivation in CAR T-cells prevents monocyte-dependent release of key cytokine release syndrome mediators. *J. Biol. Chem.* **294**, 5430–5437 (2019).
104. L. A. Madge, M. J. May, *Inflammation and Cancer* (Humana Press, 2009), pp. 209–232.

Acknowledgments: We thank A. Wang and M. Hresko for technical assistance and V. Bhoj, S. Richman, S. Ghassemi, S. Nunez-Cruz, S. Gill, T. Kambayashi, and C. van Dang for helpful discussions. We also thank S.-C. Sun for sharing the original construct from which we cloned the complementary DNA encoding dnNIK. **Funding:** This research was supported by grants from the University of Pennsylvania-Novartis Alliance (to C.H.J. and M.C.M.) and NIH grants (R01CA226983 to R.S.O. and C.H.J.; P01CA214278 to M.C.M. and C.H.J.; and R01CA172921 to S.M.A.). **Author contributions:** B.I.P., M.J.M., S.M.A., and M.C.M. designed the experiments. B.I.P. conducted the experiments. R.S.O., M.J.M., C.H.J., S.M.A., and M.C.M. provided resources. B.I.P., R.S.O., M.J.M., and M.C.M. performed formal data analysis. B.I.P. wrote the manuscript. B.I.P., R.S.O., M.J.M., S.M.A., and M.C.M. edited the manuscript. S.M.A. and M.C.M. supervised all work. **Competing interests:** C.H.J. reports receiving commercial research funding from Tmunity Therapeutics and has an ownership interest and intellectual property (IP) licensed to Novartis. M.C.M. reports receiving commercial research funding from Novartis and has an ownership interest and IP licensed to Cabaletta Bio. The other authors declare that they have no competing interests. **Data and materials availability:** All data needed to evaluate the conclusions in the paper are present in the paper or the Supplementary Materials. The anti-CD19 idiotype antibody from Novartis requires a material transfer agreement.

Submitted 21 July 2019
Resubmitted 20 October 2019
Accepted 17 March 2020
Published 31 March 2020
10.1126/scisignal.aay8248

Citation: B. I. Philipson, R. S. O'Connor, M. J. May, C. H. June, S. M. Albelda, M. C. Milone, 4-1BB costimulation promotes CAR T cell survival through noncanonical NF-κB signaling. *Sci. Signal.* **13**, eaay8248 (2020).

Science Signaling

4-1BB costimulation promotes CAR T cell survival through noncanonical NF-κB signaling

Benjamin I. Philipson, Roddy S. O'Connor, Michael J. May, Carl H. June, Steven M. Albelda and Michael C. Milone

Sci. Signal. **13** (625), eaay8248.
DOI: 10.1126/scisignal.aay8248

Ensuring the persistence of CAR T cells

Optimal antitumor responses in patients treated with chimeric antigen receptor (CAR) T cells correlates with the persistence of these cells after treatment. Confirming patient data, Philipson *et al*. found that 4-1BB–expressing CAR T cells survived longer and increased in number to a greater extent ex vivo compared to CD28-expressing CAR T cells. The 4-1BB–expressing CAR T cells exhibited enhanced noncanonical NF-κB signaling and decreased expression of apoptotic factors compared to their CD28-expressing counterparts. These findings suggest that manipulation of the noncanonical NF-κB pathway in future CAR T cell designs may provide clinical benefit.